© 2019. Published by The Company of Biologists Ltd | Journal of Cell Science (2019) 132, jcs230607. doi:10.1242/jcs.230607

RESEARCH ARTICLE

Basal-type lumenogenesis in extraembryonic endoderm stem cells models the early visceral endoderm

Minjae Kim, Yixiang Zhong, Kyoung Hwa Jung, Young Gyu Chai and Bert Binas*

ABSTRACT

Cultured rat primitive extraembryonic endoderm (pXEN) cells easily form free-floating multicellular vesicles *de novo*, exemplifying a poorly studied type of morphogenesis. Here, we reveal the underlying mechanism and the identity of the vesicles. We resolve the morphogenesis into vacuolization, vesiculation and maturation, and define the molecular characteristics and requirements of each step. Vacuolization is fueled by macropinocytosis and occurs by default if not blocked by high cell density or matrix proteins. Fine-tuned cell–cell contact then forms nascent three-cell vesicles with vacuole-derived lumina. In maturation, the vesicles complete epithelialization, expand via mitosis and continued fluid uptake, and differentiate further. The mature vesicles consist of a simple squamous epithelium with an apical-outside/basal-inside polarity that we trace back to the single cell stage. The polarity and gene expression pattern of the vesicles are similar to those of the early visceral endoderm. pXEN cells provide a useful *in vitro* model for study of matrix-independent, basal-type lumenogenesis and the physiology of the visceral endoderm.

This article has an associated First Person interview with the first author of the paper.

KEY WORDS: Stem cells, Visceral endoderm, Vacuole, Lumen, Vesicle, Polarity

INTRODUCTION

Rat primitive extraembryonic endoderm stem cells (pXEN cells) are normal, naturally immortal blastocyst-derived cell lines that show features of the primitive endoderm (PrE) and contribute exclusively to the yolk sac endoderm in chimerism experiments (Debeb et al., 2009; Lo Nigro et al., 2012). They exhibit a mesenchymal morphology under standard culture conditions (Lo Nigro et al., 2012), but undergo epithelialization when cultured on feeders (Debeb et al., 2009) or in the presence of the GSKb inhibitor Chir99021 (Chir) (Chuykin et al., 2013).

A notable characteristic of rat pXEN cell lines is their tendency to form floating multicellular vesicles *de novo* when treated with Chir under matrix-free, low-adhesion conditions (see figure S2 of Chuykin et al., 2013). Similar vesicles were obtained with mouse pXEN cells (Zhong et al., 2018), a mouse teratocarcinoma-derived visceral endoderm (VE)-like cell line (Adamson et al., 1985) and mouse embryonic stem cell-derived PrE-like cells (Anderson et al., 2017). In unpublished work, we also obtained floating vesicles with mouse XEN cells (Kunath et al., 2005), which are highly similar to pXEN cells (Zhong et al., 2018). The rat pXEN cell vesicles were never analyzed, but the vesicles from mouse cell lines were found to express markers consistent with a VE-like identity (Adamson et al., 1985; Anderson et al., 2017; Zhong et al., 2018). It thus appears that rat pXEN cell vesicles are also VE-like and that the ability to form floating VE-like vesicles is characteristic at least of rodent extraembryonic endoderm stem cell lines. However, no comprehensive gene expression or structural analysis has been performed for any of the VE-like floating vesicles and it remains possible that they exhibit artefactual features.

Floating vesicles that form *de novo* in a matrix-free environment were also reported with some other cell lines; where tested, these vesicles showed an apical-outside/basal-inside polarity (Chambard et al., 1981; Wang et al., 1990; Rivron et al., 2018), suggesting the same for pXEN cell vesicles. In contrast, vesicles that originate within an extracellular matrix (ECM) show a basal-outside/apical-inside polarity (Chambard et al., 1981; Wang et al., 1990); this vesicle type reproduces the polarity of most natural cavities and its origin has therefore been studied in detail (Datta et al., 2011; Overeem et al., 2015; Taniguchi et al., 2017; Jewett and Prekeris, 2018). The apical-outside/basal-inside polarity shown by free-floating vesicles is rare *in vivo*; a notable example is the blastocyst, the lumen of which is formed by trophoblast cells (Aziz and Alexandre, 1991). Fittingly, trophoblast cell lines easily form floating vesicles (Shimada et al., 2001; Ezashi et al., 2011; Rivron et al., 2018), making us wonder whether the equally remarkable pXEN cell vesicles also reproduce a natural polarity. Based on electron microscopy, blastocyst lumenogenesis appears to involve lysosome-associated vacuoles (Aziz and Alexandre, 1991) but, beyond this observation, the mechanisms underlying *de novo* vesiculogenesis in ECM-free environments remain unstudied.

Here, we clarify the nature and mechanism of origin of floating pXEN cell vesicles. We optimize conditions for their formation and maturation and show that the vesicular lumina exhibit a basal-type polarity. We provide arguments that this configuration is not a culture artifact, but reflects the specific anatomical and physiological relationship of the VE with the epiblast during development. As a result, we present a convenient *in vitro* model for studying basal-type lumenogenesis and the physiology of the early visceral yolk sac endoderm.

RESULTS

The central processes in vesiculation are lumenogenesis and polarization. In the present study, we first elucidated the principal mechanism of lumenogenesis by pXEN cell vesicles and then followed the evolution of cell polarity throughout this process. A potential clue to lumenogenesis was provided by our observation that pXEN cells often showed conspicuous vacuoles during routine culture. In fact, those vacuoles had previously been documented (see

Department of Molecular & Life Science, College of Science and Technology, Hanyang University (ERICA Campus), 55 Hanyangdaehak-ro, Sangrok-gu, Ansan-si, Gyeonggi-do 15588, Republic of Korea.

*Author for correspondence (bbinas@hanyang.ac.kr)

Y.Z., 0000-0003-1157-3464; B.B., 0000-0001-9631-3332

Received 7 February 2019; Accepted 28 August 2019

Journal of Cell Science (2019) 132, jcs230607. doi:10.1242/jcs.230607

movies 1 and 2 in Chyukin et al., 2013), although they were not explicitly mentioned. Similar vacuoles were seen in the closely related XEN cells (see figure 1E in Kunath et al., 2005), but not further studied. It is known that vacuoles can contribute to lumenogenesis (Aziz and Alexandre, 1991; Davis and Camarillo, 1996; Taniguchi et al., 2017), so we suspected that pXEN cell vacuoles are related to the ability of these cells to form floating vesicles. Therefore, we started this study by taking a closer look at pXEN cell vacuoles.

pXEN cells are primed to form vacuoles

We routinely maintained rat pXEN cells on fibronectin-coated plates at moderate density in the presence of several growth factors and 2% fetal bovine serum (FBS) (Lo Nigro et al., 2012) (condition A). Depending on the batch of FBS, up to 10% of the cells formed (mostly small) vacuoles. When we raised the FBS concentration to 16% (condition A plus 14% FBS), the vacuoles grew larger within a few hours and became giant after 1-2 days; higher FBS concentrations were not more effective (Fig. S1A,B). Conversely, complete removal of serum eliminated the vacuoles (Fig. S1A,B), but long term culture was not possible (data not shown). Postnatal bovine calf serum (BCS) was as effective as FBS in vacuole induction (Fig. 1A), but could not substitute for FBS in plating assays (Fig. 1B). Hence, the vacuole-inducing and mitogenic components of FBS were not identical. The plating assays also revealed that pXEN cells could not proliferate at the higher serum levels (Fig. 1B), suggesting that vacuolization interfered with proliferation. We observed similar vacuole formation in other rat pXEN cell lines, mouse pXEN cells and mouse XEN cells, but not in fibroblasts or embryonic stem cells (ESCs) (Fig. S1C). Vacuoles were also easily induced in pXEN-like cell lines established from rat and mouse yolk sacs, in primary pXEN cells emerging from cultured rat blastocysts and (less efficiently) in primary cultures of dissociated rat and mouse yolk sacs (Fig. S1C).

Extracellular regulators of vacuole formation

We wondered whether the vacuole-promoting activity of serum could be replaced by a popular serum substitute called KOSR. This was indeed the case (not shown). Moreover, the main component of KOSR, a lipid-rich bovine serum albumin (BSA) preparation (Albumax), also induced vacuoles (Fig. 1A), and this ability was retained in a >50 kDa filtrate (Fig. S1D). In contrast, BSA Cohn fraction V (BSA FV), linoleic acid–BSA and fatty acid-free BSA were ineffective (Fig. 1A, and results not shown). Thus, a BSA-bound lipid other than linoleic acid might be the active principle in the serum.

We also determined extracellular factors that counteracted vacuole formation. First, when the vacuoles were induced with FBS, they later disappeared when the cultures had reached a high cell density (Fig. S1A,B; Movie 1). Second, when cultured on feeder (rat embryonic fibroblast cell line Li1), pXEN cells did not show vacuoles despite the presence of 16% FBS (Fig. 1C). Third, several extracellular matrix molecules or preparations, including type 1 collagen, type 4 collagen, laminin, fibrin, Geltrex and fibronectin (at an increased concentration compared with condition A), inhibited vacuolization (Fig. 1C). Thus, cell–cell and cell–matrix interactions can counteract the vacuole-inducing effect of serum.

Because we knew that pXEN cells can produce collagen (Debeb et al., 2009), we tested the role of endogenous collagen production. We partially inhibited collagen synthesis and maturation with *cis*-L-hydroxy-proline (CHP) (Wang et al., 1990). Strikingly, at 0.3 mM CHP (the maximum nontoxic concentration), cells with large vacuoles, which were a small minority (10-12%; Fig. 1D; Fig. S1B) in the routine culture (condition A), now became dominant (54±6%; Fig. 1D). We obtained a similar result (28±4%) after treating the cultures with 0.1 mg/ml of collagenase 4 (Fig. 1D), showing that the CHP effect was collagen specific. Thus, in the routine culture, the intrinsic tendency for vacuolization is held in check by endogenous collagen production.

Signaling drugs can induce and inhibit vacuole formation

Next, we tested signaling drugs for their effects on vacuolization, hoping that the results would contribute to mechanistic information. Indeed, several signaling drugs induced giant vacuoles, including the GSK3b inhibitor Chir, the protein kinase C (PKC) inhibitor Bim1 and the atypical PKC inhibitor Gö6983 (Fig. 1A).

Using FBS or Chir as vacuole inducers, we tried to determine signaling pathways that would antagonize vacuolization. Because Chir is a known Wnt agonist, we first tested the Wnt/β-catenin inhibitors Xav939, IWP2 and calphostin C. However, these inhibitors did not reduce vacuole formation (Fig. S1E; IWP2 and calphostin C data not shown). In contrast, the PKC activator phorbol 12- myristate 13-acetate (PMA) blocked vacuole formation (Fig. S1E), mirroring the vacuole-inducing effect of PKC inhibitors. Additional drugs that prevented or reduced vacuole formation included forskolin (PKA activator), Y-27632 (inhibitor of ROCK, Rho-associated protein kinase), cytochalasin D (actin polymerization inhibitor), PD0325901 (MEK inhibitor), ZSTK474 (PI3K inhibitor) and imatinib (receptor tyrosine kinase inhibitor) (Fig. S1E). The effects of all of these drug were identical in both serum- and Chir-treated pXEN cells, indicating that serum and Chir induced the same type of vacuoles.

Vacuoles are nonacidic and rich in calcium

Having determined parameters that control vacuole formation, we studied the identity of the vacuoles. It is known that the VE, which blastocyst-injected pXEN cells can colonize, contains large apical vacuoles that are acidic and exhibit β-galactosidase activity (Wada, 2013; Huang and Rivéra-Perez, 2014). However, the serum-induced vacuoles of pXEN cells showed neither β-galactosidase activity (not shown) nor an acidic pH: Staining with Neutral Red or Lysotracker revealed many small lysosomes (especially in the maintenance condition), but vacuoles were stained only occasionally. Instead, vacuoles were stained green by intracellular pH Probe 1 (Lee et al., 2013), FITC-dextran and an indicator of alkaline phosphatase (AP) activity, each time implying a slightly alkaline pH (Fig. S1B,F,G). Because this appeared more typical for the extracellular milieu, we also incubated the cells with a calcium indicator dye, Fluo-3am, and observed that the vacuoles were stained intensively and selectively, indicating a high calcium concentration (Fig. S1F).

We then transfected the cells with constructs expressing fluorescently tagged organelle markers, including Sec61 (endoplasmic reticulum), Rab5 (early endosome), Rab7 (late endosome), Lamp1 (lysosome), B4galt1 (Golgi) and Cox8a (mitochondria) (Wu et al., 2016; Vashi et al., 2017; Nemani et al., 2018). None of the constructs stained the vacuoles (Fig. 1E), apart from a small proportion of vacuoles (<1%) that were stained with Lamp1, in agreement with the observations made using Neutral Red.

Vacuoles grow by macropinocytosis

In view of their rapid growth, giant size, lack of organelle markers and extracellular-like milieu, we suspected that vacuoles grow by macropinocytosis. We confirmed this using two kinds of markers: 70 kDa rhodamine B (Rho B)-dextran and 0.5 µm or 1 µm microbeads (Fig. 1F,G). In line with macropinocytosis, electron microscopy images showed abundant microvilli and membrane ruffling on the cell surface (Fig. 1H). These images also showed that the vacuoles grew to giant size by merging with smaller vacuoles

Journal of Cell Science (2019) 132, jcs230607. doi:10.1242/jcs.230607

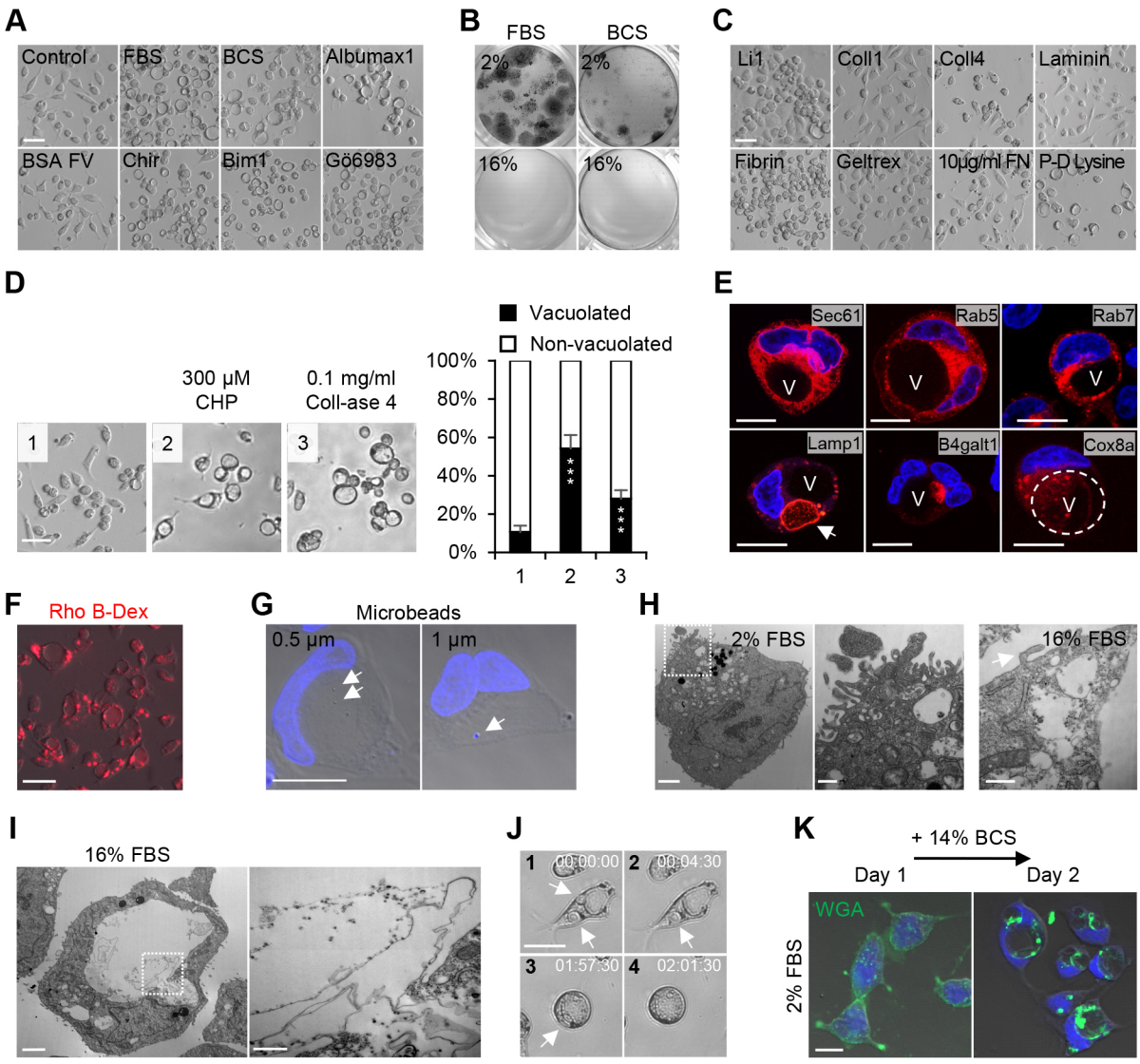

Fig. 1. Basic characterization of giant pXEN cell vacuoles. (A) Vacuole-inducing effects of different sera, albumin preparations and drugs, photographed 2 days after addition. 2500 cells/cm^2 (ground state control, 250 cells/cm^2) were seeded with additional 14% FBS, BCS, 8 mg/ml Albumax1 or BSA FV. 1250 cells/cm^2 were seeded with 0.5 µM Chir, 1 µM Bim1 or 2 µM Gö6983. (B) Plating assays under condition A but using the indicated sera and serum concentrations. 50 cells/cm^2 were plated and cultures were stained after 6 days. (C) Effects of different plate coatings on vacuolization. pXEN cells were cultured for 2 days with 16% FBS on each of the following coatings: 1.5×10^4 Li1 cells/cm^2, type 1 and type 4 collagen (commercially coated plates), 0.25 mg/ml laminin, 10 mg/ml fibrin, 0.16 mg/ml Geltrex, 10 µg/ml fibronectin (100-fold higher than the fibronectin concentration used for maintenance culture) and poly-D-lysine (P-D lysine; commercially coated plate). (D) Vacuole induction by treatment with *cis*-L-hydroxy-proline (CHP) or collagenase 4 (Coll-ase 4) for 2 days. Vacuolated and nonvacuolated cells were counted under the microscope. Mean±s.e.m. from five independent experiments (n=5). ***P<0.001 for comparison between ground state and given sample by two-tailed Student's t-test. (E) Confocal images of vacuolated pXEN cells that were genetically labeled with fluorescent organelle markers for ER (Sec61), early endosomes (Rab5), late endosomes (Rab7), lysosomes (Lamp1), Golgi (B4galt1) and mitochondria (Cox8a). The vacuoles (V) were induced with 16% FBS; outlines of some vacuoles are highlighted with a dotted line. The arrow indicates a lysosomal vacuole, which was rarely seen. (F) Vacuolar uptake of Rho B-dextran after 1 day of incubation with 14% BCS. (G) Confocal image of vacuolar uptake of 0.5 and 1 µm microbeads after 1 day of incubation with 14% BCS. Arrows indicate microbeads. (H) TEM images of pXEN cells after 1 day of incubation with 2% (left) or 16% (right) FBS. The middle photo is a magnification of the boxed region in the left photo. Note microvilli (middle photo) and plasma membrane ruffling (right photo, arrow). (I) TEM image of small vacuole merging with large vacuole 1 day after the addition of 16% FBS. Right photo is magnification of boxed region in left photo. Note that the small vacuole in turn contained vesicular material. (J) Images from Movie 2 of vacuoles merging under 14% FBS on day 1. Arrows indicate small vacuoles (time in h:min:s). (K) Translocation of surface material to vacuolar membranes. The surface membrane was pulse-labeled with CF-WGA at day 1 (2% FBS, left photo), then incubation was continued for one more day with additional 14% BCS (right). All cultures were based on condition A, and each photo represents at least two independent experiments. Coll1, type 1 collagen; Coll4, type 4 collagen. Scale bars: 0.5 µm (I right, H middle and right); 2 µm (I left, H left); 20 µm (G,K); 50 µm (A,C,D,E,F,J).

that, in turn, contained smaller membrane vesicles (Fig. 1I). The merger of large vacuoles into giant vacuoles was also directly observed in videos (Fig. 1J; Movie 2). Furthermore, when we pulse-labeled the cell surface with fluorescent CF488A-labeled wheat germ agglutinin (CF-WGA) and induced vacuolization, the vacuoles became labeled (Fig. 1K). Hence, at least in part, the vacuolar membranes were directly derived from the plasma membrane, again consistent with macropinocytosis.

Journal of Cell Science (2019) 132, jcs230607. doi:10.1242/jcs.230607

Vacuolated cells retain pXEN markers but upregulate certain GO terms and the KEGG pathways

To clarify the molecular identity of vacuolated pXEN cells, we performed RNA-seq. We compared routinely cultured (condition A or 'ground state') pXEN cells with the following vacuolated samples: (1) cultures treated with BCS (used rather than FBS because BCS lacked the proliferative effect), (2) cultures treated with Chir and (3) AP-labeled cell fraction purified from Chir-treated cultures by FACS. These vacuolated samples shared 81 upregulated and 53 downregulated genes compared with routinely cultured pXEN cells (Fig. 2A; Table S10A,B). Among the upregulated genes, the main GO terms and KEGG pathways were related to endoderm development, tubal and epithelial morphogenesis, PI3K signaling and apoptosis (Fig. 2A; Table S11A).

On the other hand, there were very few differences between the vacuolated and nonvacuolated samples with respect to early embryonic lineage markers (i.e. markers of early ICM/epiblast, PrE and trophoblast). On the heatmap, we noticed some increase in the VE marker Ihh and a decrease in the PrE marker Gata6 in Chir-treated samples (Fig. 2B). Furthermore, although not visible in the heatmap, quantitative RT-PCR revealed a tendency toward decreased PrE marker expression (especially Oct4/Pou5f1 and

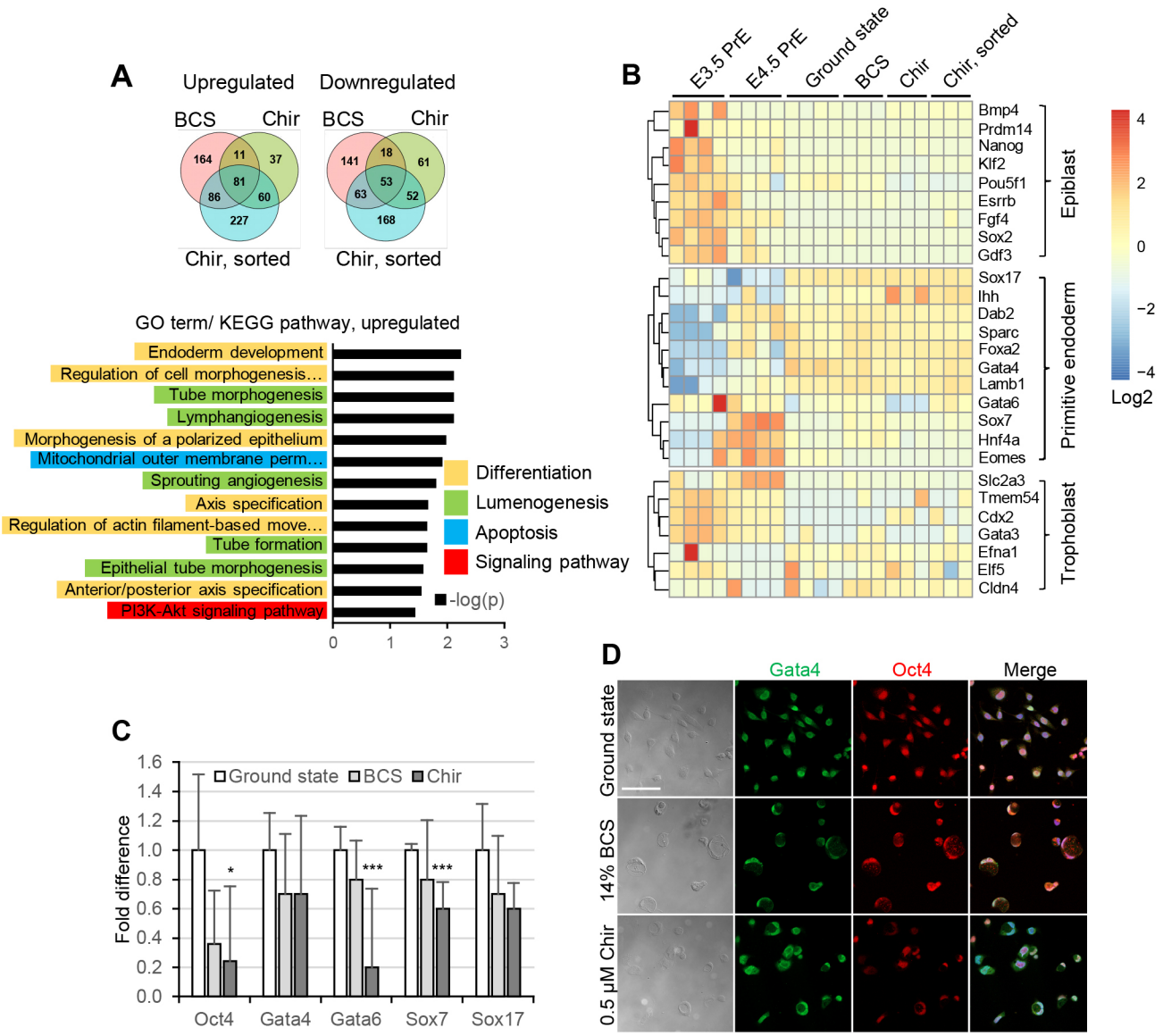

Fig. 2. Transcriptome analysis of vacuolization. (A) Upper part: Venn diagrams indicating upregulated and downregulated genes in three methods of vacuole induction: BCS, addition of 14% postnatal bovine calf serum; Chir, addition of 0.5 µM Chir; Chir, sorted, AP-stained, FACS-sorted fraction of Chir-treated cells. Lower part: GO/KEGG analysis of 81 genes upregulated in all three vacuolization conditions. Yellow bars, differentiation; green bars, lumenogenesis; blue bar, apoptosis; red bars, signaling pathways. Each circle was generated from three independent replicates by including only the shared up- or downregulated genes. See also Tables S10A,B, S11A. (B) Heatmaps comparing gene expression patterns of ground state pXEN cells (condition A with low serum), the three versions of vacuolated pXEN cells and PrE cells of E3.5 and E4.5 mouse blastocysts. Each column represents an independent replicate. (C) Confirmation by quantitative RT-PCR of RNA-seq results for selected pXEN/PrE lineage markers. Mean±s.e.m. from three independent replicates (n=3), each measured in duplicate. *P<0.05, ***P<0.001 for comparison between ground state and given sample by two-tailed Student's t-test. (D) Immunostaining for key pXEN cell markers Gata4 and Oct4 in confocal microscope. All cultures were based on condition A, modified by the addition of 0.5 µM Chir or 14% BCS. The images represent at least three independent experiments. Scale bar: 100 µm.

Journal of Cell Science (2019) 132, jcs230607. doi:10.1242/jcs.230607

to lesser degrees Gata4, Gata6, Sox7 and Sox17) in BCS- and especially Chir-treated samples (Fig. 2C). Immunocytochemistry for Oct4 and Gata4 revealed corresponding intensities (Fig. 2D).

Vacuolization leads to aberrant cytokinesis and cell death

As noticed before (Fig. 1B), pXEN cells did not form colonies when condition A was supplemented with a vacuole-inducing FBS concentration. To assess the proliferative properties of vacuolated cells, we performed additional plating assays. When transferred from routine maintenance (2% FBS) to vacuole-inducing (16% FBS) conditions, cells lost the ability to form colonies (Fig. 3A). However, when cells with giant vacuoles were plated into the routine maintenance condition, they easily formed colonies of nonvacuolated cells (Fig. 3A). Reversal to the nonvacuolated ground state was directly observed in videos (Fig. 3B; Movie 3).

In the vacuole-promoting condition, flow cytometry revealed a significant decrease in the proportion of G1 cells and a corresponding increase in the proportion of G2 cells (Fig. 3C). Live cell imaging revealed that many vacuolated cells started cytokinesis, but failed to complete it and merged back (Fig. 3D; Movie 4). The resulting binucleated vacuolated cells repeatedly tried to divide again, but finally burst (Fig. 3D; Movie 4). However, some of the vacuolated cells managed to complete cell division (Fig. 3E; Fig. S2, Movie 5). In type 1 divisions, the vacuole became a large bleb on the surface of one daughter cell and was then internalized again (Fig. 3E top; Movie 6). In type 2 divisions, both daughter cells inherited a vacuole

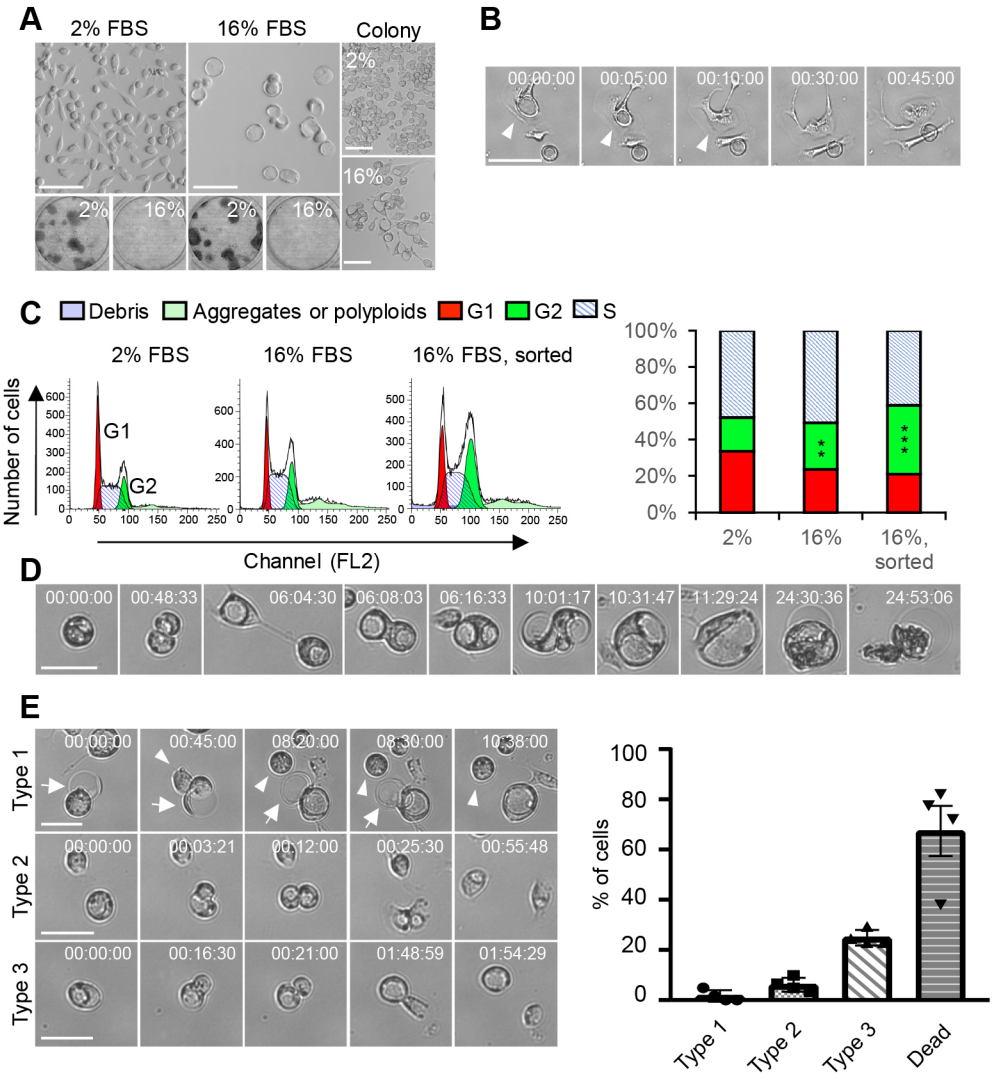

Fig. 3. Vacuolated pXEN cells exhibit a cell cycle defect. (A) Plating assays. 50 cells/cm^2 from condition A (top left) and 50 hand-picked vacuolated cells/cm^2 (induced from condition A by additional 14% FBS) (top right) (both at day 2) were plated, followed by 5 days of culture in condition A or with additional 14% FBS. (B) Live cell images (from Movie 3) indicate reversibility of vacuolated cell after change from 16 to 2% FBS (time in h:min:s). (C) Flow-cytometric cell cycle analysis of propidium iodide-stained cells after standard culture (2% FBS), after induction of vacuoles for 2 days with 16% FBS and after AP-based FACS enrichment of the vacuolated cells. A minimum of 1×10^4 to 2.5×10^4 cells were counted. $^{**}P<0.01$, $^{***}P<0.001$; comparisons between 2% FBS and given sample by the two-tailed Student's *t*-test. Mean±s.e.m. from two (16%, sorted) or four (2%, 16%) independent experiments ($n=2$ or 4). (D) Images from Movie 4 showing failed cytokinesis. This cell finally underwent cell death under 16% FBS at day 1. (E) Fates of vacuolated cells. A total of 100 dividing vacuole cells were tracked in four independent experiments using 16% FBS or 0.5 µM Chir for vacuole induction (time in h:min:s). 67.38±2.2% of cells underwent cell death as illustrated in D, the rest divided in three different ways. Left: Images from Movies 6, 7 and 8 illustrating the three types of survived cell divisions. Arrows and arrowheads indicate bleb and daughter cell, respectively. Right: Quantification of fates. Mean±s.e.m. from four independent experiments ($n=4$). All images represent at least two independent experiments. Scale bars: 50 µm (D,E); 100 µm (A,B).

(Fig. 3E middle; Movie 7). In type 3 divisions, which were the most frequent successful divisions, only one daughter cell kept the vacuole (Fig. 3E bottom; Movie 8). In summary, when vacuole-promoting conditions were maintained, most vacuolated cells unsuccessfully tried to divide and died, but some managed to complete division.

Small aggregates of vacuolated cells give rise to multicellular vesicles

Next, we determined conditions that facilitate vesicle formation. Adding Chir to the routine maintenance condition (condition A) was not effective for producing vesicles; however, vesicles formed at high frequency when (in addition to adding Chir) the serum was omitted or a low concentration of collagenase 4 (0.1 mg/ml) was added, or if cells were cultured on low-attachment plates or on the nonadhesive substrate agarose (Fig. S3A). When we simply placed the cultures on a shaker, we observed vesicle formation even in the absence of drugs, albeit at reduced frequency (Fig. S3A). Thus, low-adhesion conditions generally facilitate vesiculation.

We noticed, however, that in batch culture a complete lack of adhesion could counteract vesiculation. After treatment with a high concentration of collagenase 4 (20 mg/ml), cells floated up and formed dense multicellular aggregates (Fig. S3B). This result indicated the importance of an effective cell density; indeed, we obtained the same result by increasing cell density. We obtained vesicles in abundance by seeding 2500 cells/cm^2 on non-cell-culture grade plastic in the presence of Chir, but only large aggregates when seeding 20,000 cells/cm^2 (Fig. S3C). In 256-well agarose plates seeded with 5 cells/well, we obtained vesicles at tenfold higher efficiency than when seeding 40 cells/well (Fig. S3D). Under comparable conditions but embedded in Matrigel, single cells easily formed large colonies; however, vesicles were seen only rarely and had a very different morphology so we did not pursue this condition further.

We then explored the effects of signaling drugs on vesiculation. At least on agarose, the PKC inhibitors Bim1 and Gö6983 could substitute for Chir (Fig. S3E). On the other hand, the Chir effect was blocked by the Wnt pathway inhibitors Xav939, IWP2, and calphostin C as well as the PKA pathway stimulator forskolin, the ROCK inhibitor Y-27632 and the PKC stimulator PMA (Fig. S3E; IWP2 and calphostin C data not shown). The latter result mirrors the vesicle-inducing effect of the PKC inhibitors, indicating that Chir- and PKCi-induced vesicles are identical. Note that the Chir-antagonizing drugs had identical effects in routine maintenance medium (on agarose) and in serum-free N2B27-based medium (on low-level fibronectin) (Fig. S3E). Drugs that did not inhibit vesiculation included the MEK inhibitor PD0325901, the PI3K inhibitor ZSTK474 and the receptor tyrosine kinase inhibitor imatinib. In summary, vesiculation was most efficient when the cells were triggered to become epithelial (high concentration of Chir), were at a density favoring microaggregation and were prevented from adhering too tightly to the substratum.

How do the vacuoles fit into this scenario? To clarify this, we observed vesicle formation through time. When cells were cultured in condition B (which included 3 µM Chir) on (low-level) fibronectin, they first attached onto the dish, then floated and started to aggregate (days 5-6). Characteristically, three (sometimes four or five) vacuolated cells formed nascent vesicles by merging their vacuoles into a single lumen (Fig. 4A). Live cell imaging allowed us to observe directly the transition from vacuoles to lumen (Fig. S3F, Movies 9 and 10). Over the next month or so, the number of cells per vesicle increased and the vesicles grew to a diameter of about 1 mm (Fig. 4A); mitotic figures in DAPI-stained vesicles indicated that this involved cell proliferation (Fig. S3G). As described above for vacuoles, Rho B-dextran (70 kDa), FITC-dextran (10 kDa) and the calcium dye Fluo-3am were rapidly taken up into the vesicle lumina, suggesting pinocytosis/transcytosis and revealing a neutral to mildly alkaline pH and a high calcium concentration (Fig. S3G). Electron micrographs showed rich microvilli and membrane ruffles on the vesicle outside, plenty of vacuoles in the cytoplasm and discharges of membrane vesicles into the lumen (Fig. 4B). In summary, under low-adhesion and epithelium-promoting conditions, the vesicle lumina originated from vacuoles of three-cell microaggregates and grew by both membrane-mediated transcellular transport and an increase in cell number.

Vesicles exhibit an apical–basal polarity that can be traced to the prevacuolar stage

Electron micrographs revealed that the apical surface of the vesicle epithelia was on the outside (Fig. 4B). To obtain molecular confirmation, trace the origin of polarity and characterize the process of epithelialization, we performed immunochemistry or cytochemistry of established polarity and epithelial markers throughout the whole process of vesicular morphogenesis.

We started by co-staining for the apical membrane marker podocalyxin (Pdxl) (Bryant et al., 2014) and the basal membrane marker sodium/potassium ATPase (Na/K ATPase) (Farr et al., 2009). Even in the single cell prevacuolar ground state, Pdxl clearly marked the surface membrane and only the surface membrane (Fig. 4C). The side view revealed that only the membrane facing the medium, not the substrate-facing lower side, was positive for Pdxl (Fig. 4G,I). However, upon vacuolization, the cells often rounded up and then Pdxl marked the whole plasma membrane (Fig. S3H). In all cases, Pdxl remained strictly surface associated and never marked the vacuolar membrane. By the nascent vesicle stage, Pdxl marked the outer vesicle surface and kept doing so in the bona fide vesicle (Fig. 4C). By contrast, Na/K ATPase caused a punctuate pattern in the cytoplasm of the prevacuolar stage and was absent from the plasma membrane (Fig. S3H); however, upon vacuolization, Na/K ATPase marked the vacuolar membranes, then the luminal membranes of the nascent vesicles and eventually the luminal membrane of the vesicle itself (Fig. 4C; Fig. S3H).

Lipoprotein-related protein 2 (Lrp2, also known as megalin) is a known apical marker of the VE (Maurer and Cooper, 2005). We found it in various inner regions of prevacuolar pXEN cells without an obvious rule. However, from the nascent vesicle stage on, Lrp2 ‘condensed’ toward the outer (apical) membrane and then clearly marked the apical membrane of the true vesicles (Fig. 4D). F-actin is a cytoskeletal protein located near the apical pole in epithelia (Yano et al., 2017). Although it was seen in pseudopodia and lamellipodia of nonvacuolated and vacuolated pXEN cells, it became preferably (but not exclusively) associated with the apical side of nascent and true vesicles, and especially with regions of cell–cell contact (Fig. 4E). E-cadherin (Cdh1) is a component of epithelial adherens junctions (van Roy and Berx, 2008). It was diffusively distributed in the single cell stages (prevacuolar and vacuolar), started to condense toward the cell–cell junctions in the nascent vesicles and clearly marked cell–cell contacts (together with actin) in the true vesicle stage (Fig. 4E). Tight junction protein 1 (Zo1) is a marker of epithelial tight junctions (González-Mariscal et al., 2000). In prevacuolar and vacuolar pXEN cells, it was distributed in a somewhat punctuated pattern through the cytoplasm but became localized to the cell–cell junctions in the three-cell state and then in the mature vesicle, in a manner that overlapped with F-actin (Fig. 4F).

Journal of Cell Science (2019) 132, jcs230607. doi:10.1242/jcs.230607

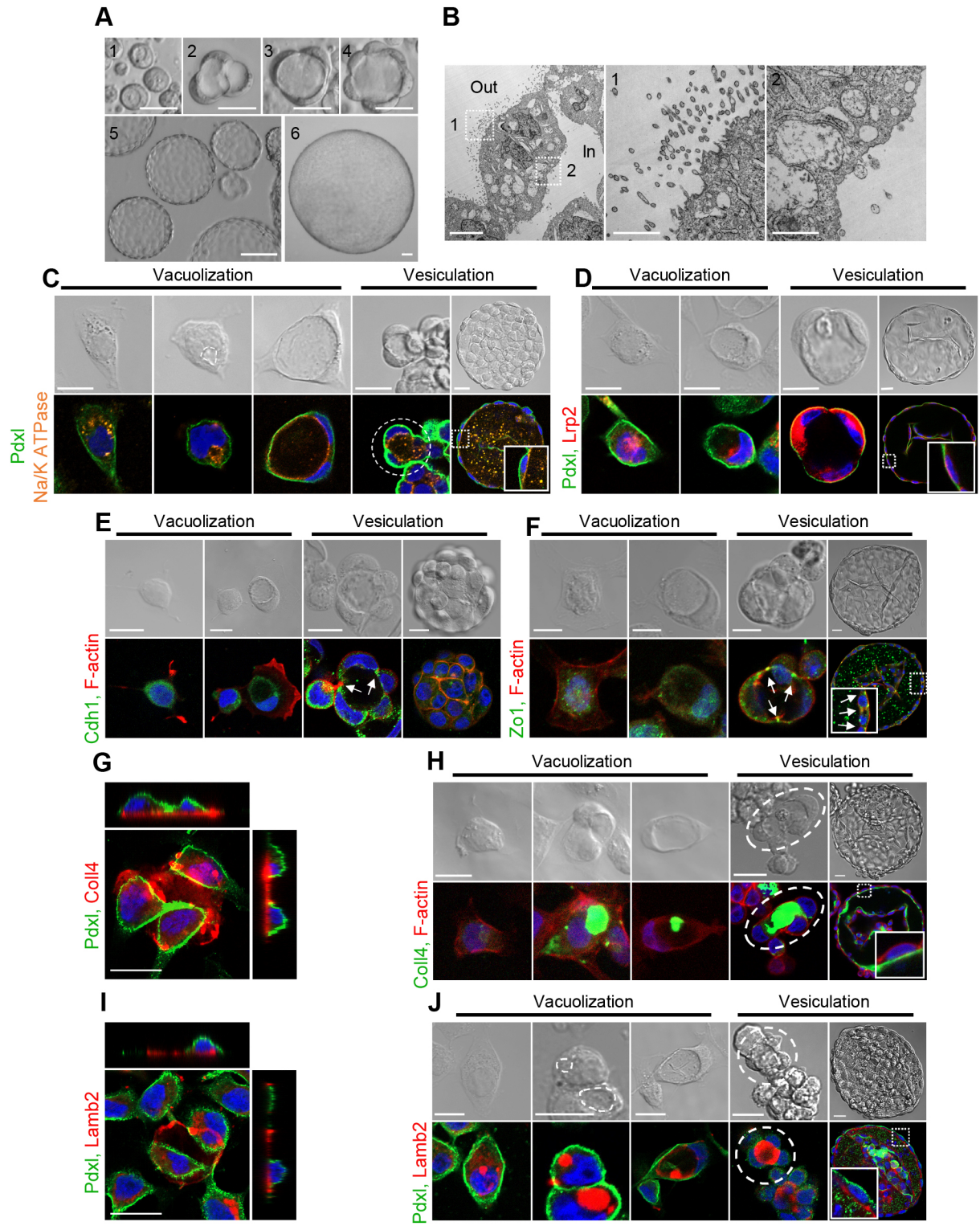

Fig. 4. See next page for legend.

Collagen 4 and laminin B2 are components of the basement membrane on which epithelia rest with their basal side (Pozzi et al., 2017). In the prevacuolar ground state, both proteins were located on the bottom of the dish, sometimes directly below the cells and sometimes in between, probably as a result of cell migration (Fig. 4G,I). Upon vacuolization, however, the two proteins appeared in the vacuoles. In a typical cell population, about a quarter of the vacuoles contained collagen and about half contained laminin (Fig. S3I). The stains were not associated with the membrane but filled the vacuoles or formed blobs (Fig. 4H,J; Fig. S3I). By the nascent vesicle stage, all lumina contained laminin and collagen, but still not in association with the membrane. In true vesicles, laminin and collagen lined the inner surface, indicating that a basement membrane had formed (Fig. 4H,J).

Fig. 4. Formation of vesicles from vacuolated cells. (A) Photoseries starting with vacuolated cells and showing typical stages (1-6) of progressive vesicle development. Stage 2 shows the nascent vesicle stage, consisting of three cells whose vacuoles are still discernable. In this example, the vesicles were formed (stages 1-4) under condition B in a fibronectin-coated four-well plate. Typically, the cells floated from the bottom at day 5 and formed microaggregates in which the vacuoles formed one central lumen. Once formed, the vesicles were transferred to an uncoated 12-well plate (stages 4, 5) where they grew to >1 mm in diameter over the next month (medium change every 2 days). (B) TEM image showing the polarity of the vesicular epithelium. Note microvilli on the outside and secretory vesicles on the inside, as well as abundant vacuoles inside the cells. Vesicles were cultured for 10 days. Boxes 1 and 2 are also shown in magnified views (middle and right). (C) Confocal images showing localization of podocalyxin (Pdxl) and Na/K ATPase through all stages of vacuolization and vesiculation. From left to right: nonvacuolated ground state cell, cell with small vacuole, cell with giant vacuole (non-lumen-forming), nascent vesicle (three-cell stage), true vesicle. (D-F) Confocal images showing expression of Pdxl and Lrp2 (D), Cdh1 and F-actin (E), or Zo1 and F-actin (F) throughout morphogenesis. From left to right: nonvacuolated ground state cell, cell with lumen-forming vacuole, nascent vesicle, true vesicle. Arrows indicate cell–cell junctions. (G) Top and side views of Pdxl and collagen 4 localization in nonvacuolated ground state cells. (H) Localization of collagen 4 and F-actin through morphogenesis. (I) Top and side views of Pdxl and laminin B2 localization in nonvacuolated ground state cells. (J) Localization of Pdxl and laminin B2 through morphogenesis. Some nascent vesicles are encircled with white dashed lines. Each photo represents at least two independent experiments, except for the electron microscopy results, which were taken from one experiment. Blue, DAPI staining. Scale bars: 0.5 µm (B middle and right); 2 µm (B left); 20 µm (C-J); 25 µm (A top row); 100 µm (A bottom row).

Together, these results show that, under routine maintenance conditions, single pXEN cells are already prepolarized in accordance with their potential epithelial fates and that pXEN cell vesicles possess all the structural elements of a true epithelium.

Multicellular vesicles exhibit features of the post-implantation visceral endoderm

To help understand the identity of the vesicles, we used RNA-seq to compare vacuolated cells and the developmental stages of the extraembryonic endoderm. Vesicles were induced by 3 µM Chir in the presence of either maintenance culture medium with 2% FBS or serum-free N2B27. Only vesicles >300 µm in diameter were collected. Compared with the vacuolated cells, both vesicle versions shared 862 upregulated and 888 downregulated genes; more up- or downregulated genes were shared than were not, indicating a high similarity of the vesicles (Fig. S4A, Table S10C,D). Among the shared upregulated genes, the dominating GO terms included epithelial differentiation, tubular morphogenesis, VE differentiation and Wnt signaling (Table S11B). On tSNE plots, the order of the ground state pXEN cells, vacuolated pXEN cells and vesicles paralleled *in vivo* differentiation: The ground state cells were horizontally aligned with E3.5 PrE, the sorted vacuolated cells with E4.5 PrE, and the vesicles with E9.5 VE (Fig. 5A). However, the heatmap of VE markers revealed a more nuanced picture. Some VE markers, such as Ihh, were increased even beyond the E6.5 level; some, like Hnf4a, were comparable; and others, such as Afp, ApoB and Ttr, were not higher than in the PrE. The early PrE markers Gata6 and Oct4 were downregulated in vesicles, whereas epithelial markers Cdh1 and Epcam were well expressed (Fig. 5B-E; Fig. S4B-C).

Overall, the picture in the vesicles was one of limited VE differentiation. We suspected that the continued presence of Chir was a limiting factor. Therefore, after the vesicles were established (within about 5-10 days), we transferred them into a Chir-free condition for 10 days and then performed quantitative RT-PCR for selected VE and epithelial markers (Paca et al., 2012; Chuykin et al., 2013). In addition, we verified two markers (Afp and Cer1) by immunostaining and stained vesicles with the lectin ligand *Dolichos biflorus* agglutinin (DBA) (Noguchi et al., 1982; Kimber, 1986). We observed a significant, in part dramatic, increase in lineage-specific VE differentiation products (especially Afp, Ttr, ApoA1, ApoB and DBA receptor), some markers of the anterior VE (Cer1, Lefty1 and Otx2) and epithelial markers (especially Ocln and Cdh1) (Fig. 5C-F). Furthermore, we noticed that the epithelial cells, which in the immature vesicles remained somewhat spindle-like, assumed a more cuboidal shape (Fig. S4D). However, we could not maintain epithelial integrity without Chir for a prolonged culture period.

DISCUSSION

pXEN cells are prestructured for self-driven, basal-type lumenogenesis

Our observations collectively indicate that, even in the ground state, pXEN cells are prestructured to form basal-type lumina in a self-driven process.

First, we found that routinely cultured pXEN cells (i.e. disconnected cells with a ‘mesenchymal’ appearance) showed signs of an apical–basal polarity. That is, even though many cells exhibited front–rear polarity (as demonstrated by morphology and actin staining), the medium-facing membranes of all cells (regardless of morphology) were exclusively stained for the apical marker Pdxl, but not for the basolateral marker Na/K ATPase. Importantly, these membranes continuously remained positive for Pdxl until they became the outer (apical) membranes of the vesicles. This is a difference from the well-studied process of apical-type lumen formation by MDCK cells, which initially also contain Pdxl in the outer membrane, but then relocate it to the cell–cell contact region at the end of the first cell division (Bryant et al., 2014). It is also different from a kind of apical-type lumen formation by endothelial cells, where Pdxl is recruited to the cell–cell contact region from intracellular locations (Strilić et al., 2009).

Second, ground state pXEN cells showed an intrinsic tendency toward vacuolization. We exposed this tendency by inhibiting collagen production with CHP, which implies that the cells have to suppress vacuolization actively in order to maintain their ground state. The collagen specificity of this effect was supported by the observation that treatment with collagenase also stimulated vacuolization. Because various exogenously added matrix proteins (including collagen) were also able to block vacuolization (when it was ‘induced’ by serum), it appears that cell–matrix interaction in general antagonizes vacuolization.

Third, the properties of vacuoles pre-empted their destiny as the lumen of the vesicles. That is, the vacuolar contents appeared similar to the extracellular milieu, and the vacuolar membranes already showed the polarity that corresponded to their fate as a luminal membrane (i.e. basal polarity; staining for Na/K ATPase but not Pdxl). The basal-luminal fate of the vacuoles was further in line with the accumulation of laminin and collagen, two key components of the future basement membrane. Importantly, however, the intravacuolar accumulation of collagen and laminin followed, rather than preceded, membrane polarization and these proteins were not initially associated with the vacuolar membrane. Hence, although both collagen and laminin can induce polarization and (apical-type) lumenogenesis in epithelial cells (Lee and Streuli, 2014; Overeem et al., 2015), they do not seem to play this role in pXEN cells. Of course, this does not exclude the possibility that the intraluminal ECM proteins later reinforce polarization once they had formed a basement membrane. We speculate that the matrix-independent polarization of pXEN cells avoids a conflict resulting from the ability

Journal of Cell Science (2019) 132, jcs230607. doi:10.1242/jcs.230607

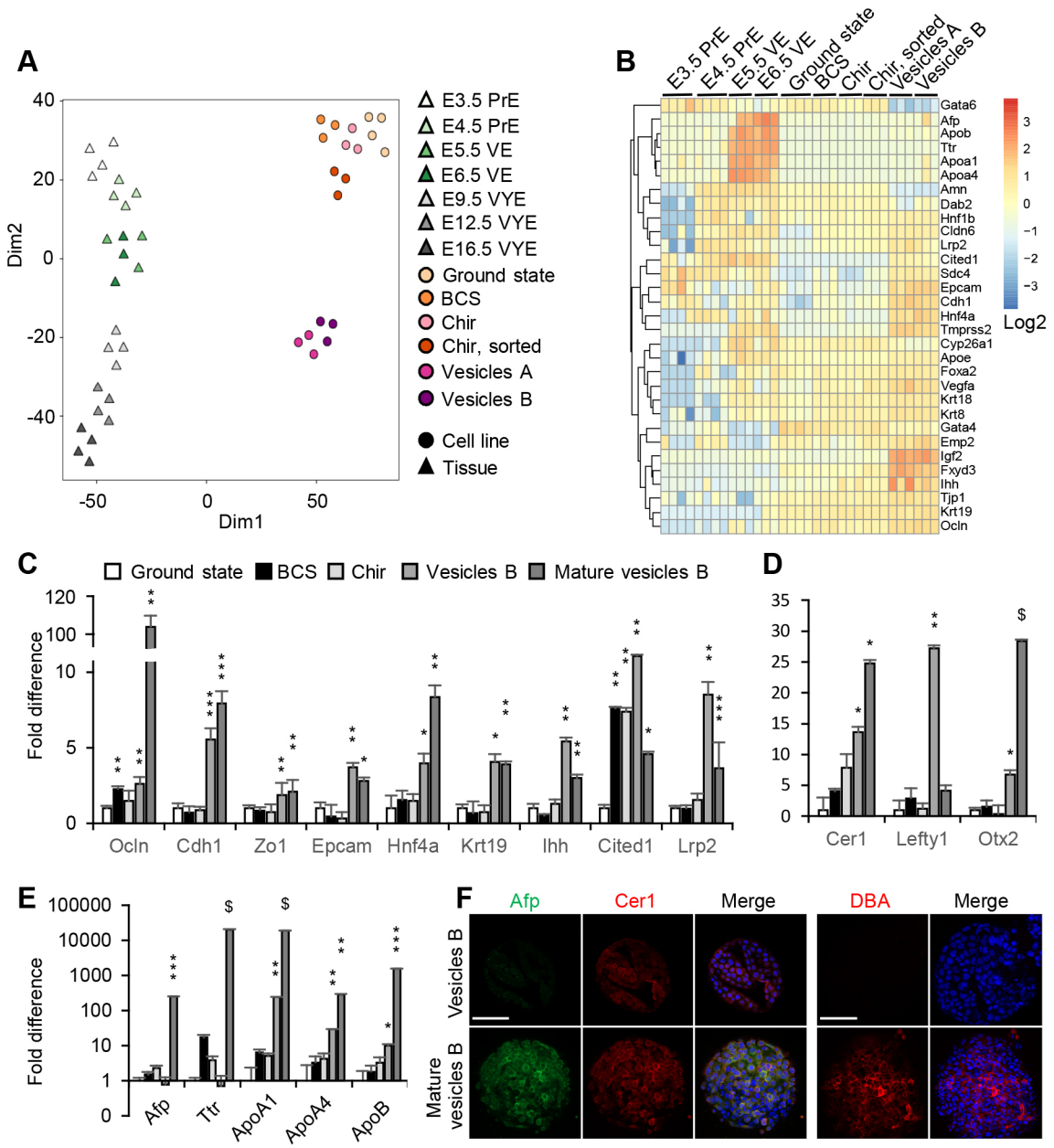

Fig. 5. Visceral endoderm-like differentiation of vesicles. (A) tSNE plot of pXEN cells, pXEN cell-derived *in vitro* morphotypes and related *in vivo* cell types. Vesicles were prepared in condition A (vesicles A) or B (vesicles B), each supplemented with 3 µM Chir. (B) Heatmap comparison of VE marker expression by the same cell types as in A. (C) Verification of VE marker expression by quantitative RT-PCR. (D) Quantitative RT-PCR revealing vesicular expression of anterior and distal VE markers not found by the RNA-seq. (E) Dramatically increased expression of selected VE markers in mature vesicles. Mean±s.e.m. from three independent replicates (n=3), each measured in duplicate. (F) *In situ* detection of mature VE markers, Afp and DBA, in mature vesicles also showing Cer1 expression. Vesicles were produced in condition B for 5-10 days (vesicles B), then cultured in condition C without Chir for an additional 10 days (mature vesicles B). Images were taken under a confocal microscope. Each photo represents at least two independent experiments. Scale bars: 100 µm. *P<0.05, **P<0.01, ***P<0.001, $^{\$}P$<0.0001 for comparisons between ground state and given sample by two-tailed Student's t-test.

to secrete collagen and laminin both on the cell surface and into the vacuoles. Indeed, the ground state pXEN cells also deposited collagen and laminin below their bottom membrane (which, however, did not contain the basal membrane marker Na/K ATPase).

Titrated cell–cell contact triggers vesiculation

For the vacuolization to progress into vesiculation, a finely adjusted cell–cell contact is key. At low cell density (i.e. in the absence of cell–cell contact), the vacuoles grew to giant size, which disrupted cytokinesis and the cells died. This was reminiscent of the previous observation of giant vacuoles with basolateral characteristics in the trophectoderm of blastocysts when cell–cell contact was compromised by knockout of Cdh1 (Stephenson et al., 2010). At the opposite extreme (i.e. at high cell density), pXEN cell vacuoles did not form or they reverted, because cell–cell contact counteracted vacuolization. However, a balance was reached at a certain intermediate density. In very small cell aggregates, three to five (typically three) appropriately positioned cells undergoing vacuolization formed cell–cell junctions containing Cdh1 and Zo1, which allowed the vacuoles to extrude their contents into a

diffusion-restricted intercellular space. This mode of lumen initiation fits the mechanism of intracellular hollowing, perhaps with some cord hollowing, as previously seen in endothelial cells (Sigurbjörnsdóttir et al., 2014). At this nascent vesicle stage, F-actin and Lrp2 became associated with the apical pole, whereas collagen 4 and laminin started to associate with the basal pole. Interestingly, although the ECM was able to prevent vacuolization and morphogenesis, a complete lack of substrate adhesion (e.g. high concentration of collagenase) tended to let the cells float up too easily, which favored the formation of multicellular aggregates that did not produce vesicles. Very gentle adhesion provided an anchor that helped the cells in the microaggregates to interact. Hence, cell–substrate adhesion was clearly not an initiator of lumenogenesis, but could support it in a subtle way.

Once formed from only three to five cells, the vesicles expanded, which required a simultaneous increase in both luminal volume and cell number. Interestingly, the experiments with labeled FITC-dextran, calcium imaging and electron microscopy suggest that the same process that drove vacuolization (namely, pinocytosis) became extended into performing transcellular transports to support the volume increase. At the same time, the discharge of vacuolar contents into the growing lumen prevented the deadly vacuole gigantism, thus allowing the cell cycle to continue (as evidenced by mitoses). The near inability of single vacuolated pXEN cells to divide might also prevent the start of lumenogenesis from the two-cell stage, indicating another difference from the lumenogenesis of MDCK cells.

Taken together, our results reveal that pXEN cells are prepolarized and prestructured for basal-type lumenogenesis and do not depend on the classical inducers, cell-matrix or cell–cell interaction (Lee and Streuli, 2014; Sigurbjörnsdóttir et al., 2014; Manninen, 2015; Overeem et al., 2015; Ebnet et al., 2018) to trigger this process. Rather, they start the first stage of lumenogenesis (vacuolization) by default once an inhibitor is removed. Interestingly, this inhibitor is the ECM (endogenous collagen or exogenous ECM) (Fig. S5A). In contrast, the second stage (vesiculation) of vesicular morphogenesis requires a positive trigger, namely a finely adjusted cell–cell interaction, which leads to lumen initiation, epithelialization and mitosis. In this second stage, the vacuole mechanisms still operate but in controlled form, supporting expansion of the vesicles.

Future work must underpin the above mechanism with molecular details such as the surface receptors, intracellular transport and signaling pathways involved. As to the latter, our drug experiments so far suggest that the vacuolization stage is under the control of PI3K signaling, whereas the vesiculation stage appears to be controlled by Wnt signaling (Fig. S5B).

Parallels between pXEN cell vacuoles and apicosomes

Because of the close anatomical, developmental and, consequently, physiological relationship between VE and epiblast, we found it interesting to compare pXEN cell vacuoles with the recently described apicosomes of epiblast stem cells, which create an *in vitro* equivalent of the pro-amniotic cavity (Taniguchi et al., 2017). In egg cylinder stage embryos, epiblast and VE (represented by pXEN cell-derived multicellular vesicles) are sandwiched and their basal sides face each other (Bielinska et al., 1999).We showed that, like apicosomes, pXEN cell vacuoles lack standard organelle markers, exhibit a nonacidic pH, contain calcium ions at a high level, derive their membranes from the plasma membrane, grow by macropinocytosis and contribute to vesicular morphogenesis by providing the luminal membrane and fluid. Moreover, both vacuolated pXEN cells and apicosome-containing epiblast stem cells exhibited signs of basal–apical polarity at the single cell stage, albeit in opposite orientations. Thus, apicosomes and pXEN cell vacuoles might be two variants of the same lumenogenic organelle, distinguished by the orientation of their polarity. It will therefore be interesting to compare these organelles in more detail. An obvious difference is that apicosomes are associated with a primary cilium, which pXEN cells almost certainly lack (Bangs et al., 2015).

pXEN cell vesicles as a three-dimensional model of the early visceral endoderm

As mentioned in the Introduction, basal-type lumenogenesis is not the norm in mammals. So, do pXEN cell vesicles represent the natural polarity of the VE? We argue that, in this specific case, it depends on what is being studied. Unusual for an epithelium, the early VE can be viewed as part of two vesicular ‘organs’, the yolk sac with its yolk sac cavity and the egg cylinder with its pro-amniotic cavity (Fig. S6, left). Hence, VE vesicles with apical-type lumina are more representative of the yolk sac, whereas VE vesicles with basal-type lumina (present study) should be more representative of the egg cylinder (Fig. S6, right).

In vivo, the VE probably works in tandem with the epiblast. The epiblast creates, in a noncavitational process, the pro-amniotic cavity (Bedzhov and Zernicka-Goetz, 2015). Anatomically, it seems inevitable that the necessary fluid enters through the VE layer. However, although moving overall in one direction (from the yolk sac cavity toward the pro-amniotic cavity), fluid transport must go from apical to basal in the VE, but from basal to apical in the epiblast. This could occur in both cell types through similar mechanisms, involving apicosomes in the epiblast (Taniguchi et al., 2017) and oppositely polarized equivalents in the VE. It seems reasonable to expect that VE vacuoles are similar to pXEN cell vacuoles, as the latter are similar to apicosomes (present study) and transcellular transport in pXEN cell vesicles is probably the extension of the vacuole-based vesicle-forming mechanism(s) (supported by the experiments with labeled dextran, calcium imaging and electron microscopy). In further support, in nascent and growing vesicles we observed the expression of Lrp2 and Dab2, which have been associated with transcytosis in the VE (Maurer and Cooper, 2005).

Vacuoles have been observed in the VE at the egg cylinder stage. However, they usually are considered to be of the acidic (lysosomal) type (Kawamura et al., 2012; Wada, 2013; Huang and Rivéra-Perez, 2014), whereas apicosomes and pXEN cell vacuoles are not acidic. Most probably, the vacuolar population within VE cells is complex; even in vacuolated pXEN cells, we occasionally observed acidic vacuoles along with the nonacidic ones (for an example, see Fig. 1E, Lamp1). Regardless of whether lysosomes participate in fluid transcytosis, as might be the case in blastocysts (Aziz and Alexandre, 1991), our experiments with FITC-dextran confirmed that the lumina of our vesicles were not acidic. It will therefore be of interest to compare the vacuolar populations of pXEN cell vesicles and the VE.

We cannot advocate our pXEN cell multicellular vesicles as an ‘egg cylinder-type’ model of the VE without considering their gene expression patterns. Here, we characterize for the first time the whole gene expression spectrum of the vesicles. The data indicated a close similarity with the early VE, and we observed an even higher expression of differentiated VE markers when we withdrew Chir from the established vesicles. Notably, we saw a dramatic induction of Afp, Ttr and DBA staining and a significant increase in ApoA1, ApoA4 and ApoB, which all are well-established VE markers.

Thus, pXEN cell vesicles with basal-type lumina provide an opportunity to study developmental and physiological aspects of the early VE in isolation. The apical-outside/basal-inside polarity of

Journal of Cell Science (2019) 132, jcs230607. doi:10.1242/jcs.230607

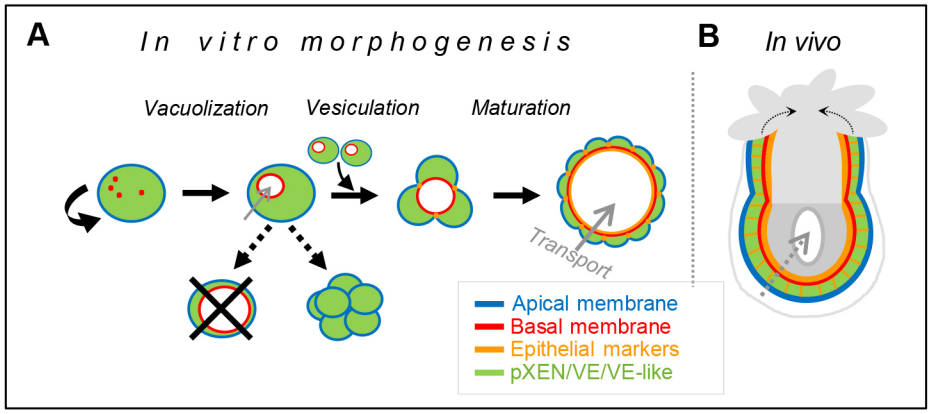

Fig. 6. Morphogenesis of pXEN cell vesicles and their proposed *in vivo* correlate. (A) Flow diagram of *in vitro* morphogenesis. Blue, red and orange colors denote the positions of tested proteins from the time point when these mark a polarity or the epithelial state (this is not identical with gene expression). The green color denotes lineage markers. Vacuolization: Self-renewing pXEN cells exhibit apical marker on their outer membrane. Removal of an ECM-caused block (Fig. S5A) allows pinocytosis-driven default basal-type vacuolization to go ahead, and self-renewal stops. If cell density becomes too high, large aggregates form in which the vacuoles disappear; if cell density is too low, the vacuoles grow to giant size and kill the cells. Vesiculation: At an appropriate intermediate cell density, configurations of three to five cells form epithelial cell–cell junctions that allow the vacuoles to discharge their contents into a restricted intercellular space. Maturation: A basement membrane forms. Continued pinocytosis feeds transcytosis, driving luminal expansion and (by preventing vacuolar growth) allowing mitosis to continue. Grey arrows indicate pinocytotic fluid transport that first feeds the vacuoles, then the vesicles. (B) Egg cylinder stage embryo. Grey areas indicate epiblast (lower part, darker gray; with pro-amniotic cavity in the middle) or trophoblast (upper part, lighter gray); the other colors have the same meaning as in A. We postulate that VE and epiblast operate in tandem to feed the pro-amniotic cavity by pinocytotic fluid transport.

this model should be particularly useful for studying the transport of molecules and fluid related to the nutritional role of the visceral yolk sac and its support of the epiblast.

Conclusions

We present three main conclusions: (1) pXEN cells provide an excellent model for dissecting the poorly understood basal-type lumenogenesis. We resolved this process into molecularly defined stages and determined the principal cellular mechanism (Fig. 6A). We found that single pXEN cells are remarkably prestructured for this process, which proceeds in a self-driven manner but is controlled by ECM and cell–cell contact (Fig. S5A). (2) Our results suggest that pXEN cell vacuoles (this study) and apicosomes (Taniguchi et al., 2017) together define a class of organelles that play important roles in the generation and expansion of lumina, but exist in alternative polarities. We propose that these organelles operate in tandem in the VE and epiblast, respectively (Fig. 6B). (3) The *in vivo*-like polarity and VE-like differentiation of pXEN cell-derived multicellular vesicles make them attractive for studying the physiology of the early visceral yolk sac endoderm *in vitro* (Fig. 6; Fig. S6). The relevance of this model is emphasized by the fact that pXEN cells can contribute to the VE *in vivo* (Debeb et al., 2009).

MATERIALS AND METHODS

Cell culture media, additives and drugs

Key cell culture materials included Albumax1 (11020-021; Thermo Fisher Scientific, Waltham, MA, USA), bovine fibronectin (Thermo Fisher Scientific, 33010018), BCS (S003-05; Welgene, Gyeongsan, Korea), B27 without vitamin A (Thermo Fisher Scientific, 12587-010), FBS (2916754; MP biomedicals, Santa Ana, CA, USA), Glutamax (Thermo Fisher Scientific, 35050061), KOSR (Thermo Fisher Scientific, 10828-010), low glucose DMEM (D6046; Sigma-Aldrich, St Louis, MO, USA), DMEM/F12 (Thermo Fisher Scientific, 21331-020), Neurobasal (Thermo Fisher Scientific, 21103-049), N2 (Thermo Fisher Scientific, 17502-048), penicillin/streptomycin (Thermo Fisher Scientific, 10378016), trypsin/EDTA (Welgene, LS015-09), β-mercaptoethanol (Sigma-Aldrich, M7522).

Drugs used included bisindolylmaleimide1 (Bim1) (B-6191; LC Laboratories, Woburn, MA, USA), calphostin C (AG-CN2-0430-C100; Adipogen, San Diego, CA, USA), *cis*-L-hydroxy-proline (H1169; Tokyo chemical, Nihonbashi-honcho, Tokyo, Japan), Chir99021 (4423; Tocris, Bristol, UK), collagenase 4 (LS004186; Worthington, Lakewood, NJ, USA), forskolin (Tocris, 1099), Gö6983 (LC Laboratories, G-7700), imatinib (LC Laboratories, I-5508), IWP2 (6866167; Peprotech, RI, USA), PD0325901 (Tocris, 4192), phorbol 12-myristate 13-acetate (PMA) (LC Laboratories, P-1680), Y-27632 (A3008; Apexbio, Boston, MA, USA), Xav939 (13596; Cayman, Ann Arbor, MI, USA) and ZSTK474 (S1072; Selleck, Houston, TX, USA).

For a complete list of media, additives and chemicals see Tables S1, S2.

Cell lines

The blastocyst-derived rat pXEN cell lines have been previously described (Debeb et al., 2009; Lo Nigro et al., 2012). pXEN-like yolk sac stem cell lines were derived from yolk sacs as follows: Yolk sacs (E10.5, mouse; E11.5, rat) were minced with scissors and incubated with 1 ml of 0.05% trypsin/EDTA in a 37°C water bath for 1 h and then washed with DMEM containing 10% (v/v) FBS and 1% (v/v) penicillin/streptomycin. The pXEN and pXEN-like cell lines were maintained as previously described (Lo Nigro et al., 2012) at a low density on fibronectin-coated plates in medium containing a low (2%) concentration of FBS; we refer to this as condition A, and to the pXEN cells as being in a 'ground state' (the culture conditions used in this study are summarized in Table S3). Mouse XEN cell lines (Kunath et al., 2005; Debeb et al., 2009), the rat feeder cell line Li1 (Debeb et al., 2009) and the mouse ESC line HM1 (Magin et al., 1992) were maintained as previously described. All cell lines used in this study, except for the ESCs, were derived in our laboratory (see Tables S4, S5). Using DAPI (Sigma-Aldrich, D9542) staining and confocal microscopy, we ascertained that our cell lines were free of mycoplasma contamination.

pXEN cell lines carrying fluorescent organelle markers were generated by separately transfecting the following constructs obtained from Addgene (Watertown, MA, USA): B4GALT1-pmTurquoise2 (Golgi, 36205), Lamp1-RFP (lysosomes, 1817), Sec61-mCh (ER, 49155), Rab7-GFP (late endosomes, 12605), Rab5-mRFP (early endosomes, 14437) and COX8A-pmTurquoise2 (mitochondria, 36208); see Table S6 for more details. Then, 1 µg of the given plasmid in 50 µl NaCl and 1 mg/ml polyethylenimine (23966; Polyscience, Warrington, PA, USA) in 50 µl NaCl were mixed, incubated for 10 min at room temperature and added to the cells. On the next day, cells were washed three times with PBS and incubated in fresh medium containing 1 µg/ml puromycin (ant-pr-1; Invivogen, Pak Shek Kok, Hong

Kong) for 3-4 days, after which colonies were collected. Confocal images were obtained with a Zeiss LSM 800 confocal microscope (Carl Zeiss, Oberkochen, Germany) using a 63× objective.

Experimental treatments

Induction and inhibition of vacuoles

pXEN or pXEN-like cells were seeded (day 0) into four-well plates at 2500 cells/cm^2 and cultured for 2 days as in condition A, but with the additional presence of a vacuole inducer. The kinds and concentrations of the inducers used are specified in the figure legends. To characterize the vacuole-inducing activity of serum, FBS was centrifuged (4000×***g***) through a 50 kDa filter (UFC805008; Merck Millipore, Burlington, MA, USA) for 15 min at 4°C. Mouse XEN cells (in their routine culture condition) were supplemented with an additional 20% FBS, resulting in a serum concentration of 30%.

When testing drugs for their vacuole-inhibiting ability, they were added on day 1 (1 day after seeding the cells) and the experiment terminated on day 2. In these experiments, either Chir or FBS was used as inducer and was added on day 0 or day 1, respectively. To test the effect of cell–cell contact, vacuoles were induced by FBS (added on day 0) and the proportion of vacuolated cells was quantified at specified time points by flow cytometry. To test the effects of different culture substrates, cells were seeded in condition A but with modified coating and the additional presence of 14% FBS (added on day 0); the culture was continued for a further 2 days. Coatings included type 1 collagen (39024; SPL, Pocheon, Korea), type 4 collagen (SPL, 39424), laminin (Thermo Fisher Scientific, 23017015), poly-D-lysine (SPL, 39224), 10 µg/ml fibronectin, 10 mg/ml fibrin (SC-473503; Santa Cruz Biotechnology, Dallas, TX, USA), 0.16 mg/ml Geltrex (Thermo Fisher Scientific, A1413201) and 1.5×10^4 mitomycin C (Tocris, 3258)-treated Li1 cells/cm^2.

Induction, differentiation and inhibition of vesicles

To induce vesicles, rat pXEN cells were subjected to one of the following five procedures: (1) 2500 cells/cm^2 were cultured under condition B, defined as follows: DMEM/F12, Neurobasal, N2, B27 without vitamin A, 1% penicillin/streptomycin, 1% (v/v) Glutamax, 100 µM β-mercaptoethanol, 10 ng/ml LIF (01-A1140; ORF Genetics, Kopavogur, Iceland) in four-well plates coated with 100 ng/ml bovine fibronectin and additionally supplemented with 3 µM Chir. In some cases (RNA-seq and immunostaining experiments), the vesicles were transferred into 12-well plates for further growth (typically for ∼5 days). (2) On day 0, cells were seeded as in condition A, but into 256-well microwell plates (ten cells/well). After 30 min (when the cells had settled down), an additional 800 µl of the same medium was added. On day 1, the vesiculation-promoting drug was added (3 µM Chir, 3 µM Bim1 or 5 µM Gö6983) and the culture terminated 3-4 days later. In some cases (RNA-seq experiments), the vesicles were transferred into 12-well plates for further growth (typically for ∼5 days). The microwell plates were prepared on day −1 by pouring 3% agarose (50004; TAKARA, Kusatsu, Japan) in water into a silicone mold (Sigma-Aldrich, Z764000). After 10 min, the agarose plate was transferred into a 12-well plate and 1 ml of condition A medium was added; the plate was then transferred into the incubator. On the following day (day 0), the medium was replaced with 1 ml of condition A medium containing the cells. (3, 4) Cells were plated at 2500 cells/cm^2 in regular (3) or low attachment (4) (SPL, 39706) four-well plates in condition A, but without FBS. Inhibitors were added as in procedure 2. (5) The pXEN cells were pre-aggregated in agarose microwells (50 cells/well seeded) for 3 days and then transferred to a 12-well plate on a shaker (5-10 days, condition A but without fibronectin).

To differentiate vesicles, they were first produced by procedure 1 and then transferred into condition C, defined as Advanced DMEM/F12 (Thermo Fisher Scientific, 12634-010), N2, B27 without vitamin A, 1% penicillin/streptomycin, 1% (v/v) Glutamax, 1.25 mM *N*-acetylcysteine (Sigma-Aldrich, A7250), 500 nM A83-01 (Peprotech, 9094360) and 50 ng/ml EGF (130-093-825; Miltenyi Biotec, Bergisch Gladbach, Germany). Cells were cultured for another 10 days in the absence of Chir.

For inhibition of vesicles, inhibitors were added on day 4 during procedure 1 or on day 3 during procedure 2 (with 3 µM Chir) and incubated for 1-2 days.

Note that several (but not all) conditions (e.g. condition A plus Chir) were able to support the entire morphogenesis from the ground state to the true vesicle, but with different efficiencies for individual steps. If not stated otherwise, we used the optimal condition for each step: A for the ground state and B for the three-cell stage and vesicles. Vacuoles were originally induced with A plus 14% serum but later more often with A plus 0.5 µM Chir (both conditions created the same type of vacuoles; see section 'Signaling drugs can induce and inhibit vacuole formation').

Analytical methods

Endo- and transcytosis assays

Three types of assays were used: (1) Cells or vesicles, in four-well plates, were incubated with FITC-dextran (Sigma-Aldrich, FD10S) or Rho B-dextran (Sigma-Aldrich, R9379) (40 µg/ml each) for 6 h on day 2 (vacuole experiments) or day 5 (vesicle experiments), followed by a medium change. Living cells were observed with an inverted fluorescence microscope (DMIL LED/DFC295, Leica Microsystems, Wetzlar, Germany) with a 10× or 20× objective. (2) Microbeads (3.64×10^7 of 1 µm or 0.5 µm; Polyscience, 19391-10 and 15700-10, respectively) were added to vacuolated cells on day 1. On day 2, the cells were washed with PBS three times and fixed for 15 min with 4% paraformaldehyde at pH 7.4 (58295-1201; JUNSEI, Tokyo, Japan); nuclei were then stained with 4 µg/ml DAPI for 10 min. (3) CF488A-labeled wheat germ agglutinin (CF-WGA) (4 µg/ml; 29022-1; Biotium, Fremont, CA, USA) was added to vacuolated cells for 10 min at 37°C and the cells were washed, fixed and DAPI-stained immediately or, after a medium change, 1 day later. An LSM 800 Zeiss confocal microscope with a 63× or 40× objective was used for the microbeads or WGA experiments. In assays 1 and 2, vacuoles were induced with FBS and in assay 3 with either Chir or FBS (with identical results). In assay 1, vesicles were induced using vesicle induction procedure 1.

Inhibition of collagen production and degradation of collagen

Vacuoles were produced over 2 days in condition A plus 0.5 µM Chir in the absence or presence of either 300 µM *cis*-L-hydroxy-proline (CHP) or 0.1 mg/ml collagenase 4. Vesicles were formed over 5 days in condition B in the absence or presence of 20 mg/ml collagenase 4. A Leica inverted fluorescence microscope with 10× objective was used.

Assessment of vacuolar or luminal pH and calcium imaging

Vacuoles were prepared in condition A plus 14% FBS over 2 days; vesicles were prepared in condition B over 5 days. After this time, while still in the incubator, vacuoles and vesicles were labeled with the indicated dyes as follows: 4 µg/ml Neutral Red (Sigma-Aldrich, N7005) for 10 min; 1 µM lysotracker (Thermo Fisher Scientific, L12492) for 30 min; 40 µg/ml FITC-dextran for 6 h; 20 µM Probe 1 (pH indicator) (Lee et al., 2013) (the kind gift of Prof. Chulhun Kang, Kyung Hee University, Korea) overnight; and 4.5 µM Fluo-3am (C213; ABP Biosciences, Beltsville, MD, USA) for 1 h. Before photography, cells were washed three times with PBS, except for calcium imaging, where the medium was changed to fresh medium and the incubation continued for an additional 20 min. Images were taken with a Leica inverted fluorescence microscope using a 20× (for vacuoles) or 10× (for vesicles) objective.

Plating assays

Cells were plated at 50 cells/cm^2 and cultured for 6 days under the conditions specified in the figure legends. They were then photographed with a 2.0 MP USB digital microscope (Digitech industries, Sheung Wan, Hong Kong) and the colonies counted.

Quantitative assessment of vacuolization

We determined the percentage of vacuolated cells by visual count or flow cytometry. For the visual count, about 1000 cells total for each data point were counted in five independent experiments directly in the culture dish with an inverted phase contrast microscope (10× objective). For flow cytometry, the cells were trypsinized and stained with 0.1 µM alkaline phosphatase (AP) live stain dye (Thermo Fisher Scientific, A14353) in 500 µl low-glucose DMEM for 30 min (see photo in Fig. S1B), then immediately run without a washing step through a Becton Dickinson

FACSCalibur device (BD Biosciences, San Jose, CA, USA). Because the dye tended to leak out again, we limited the run time per sample to ∼1 min (∼80,000 cells). Up to ten samples were run in one comparison (∼10 min total). In this time frame, the AP dye did not significantly leak out, as confirmed by running the same samples a second time with the same result. Where applicable, both methods gave equal results in direct comparison.

Cell cycle analysis

Trypsinized cells were resuspended in ice cold 70% ethanol for 1 h at 4°C, washed once with PBS and then resuspended in 500 µl propidium iodide solution (10 µg/ml; Sigma-Aldrich, P4170) in PBS containing 0.1% Triton X-100 (T/3751/08; Thermo Fisher Scientific, Hampton, NH, USA) and 100 µg/ml RNAse A (43014; m.biotech, Hanam, Korea) and analyzed immediately (∼80,000 cells per run) or stored at 4°C. A FACSCalibur device was used for the analytical runs. Cell cycle analysis was performed with ModFit LT software (Verity Software House, Topsham, ME, USA).

Immunostaining

To stain adherent cells, they were cultured in four-well plates and fixed with 4% paraformaldehyde (pH 7.4) for 15 min, permeabilized with 0.1% Triton X-100 in PBS for 15 min, rinsed three times with PBS and incubated for 1 h in blocking solution of 5% donkey serum (GTX73205; Genetex, Irvine, CA, USA) in PBS. Cells were then incubated with the primary antibody (in blocking solution) overnight at 4°C, washed three times for 5 min each with blocking solution and incubated for 1 h with the secondary antibody (1:200 in blocking solution). The antibody-stained cells were incubated with DAPI for 10 min, rinsed three times for 5 min each with blocking solution and mounted in Vectashield (H-1000; Vector Laboratories, Burlingame, CA, USA) for 10 min. For nonadherent samples (nascent vesicles and vesicles), the same procedure was followed, except that the samples were handled using a glass Pasteur pipette (D-34323; Hilgenberg, Rheinstetten, Germany). Except for the primary antibody incubations, all procedures were performed at room temperature. Antibodies and their dilutions are listed in Table S7. Images were obtained with a Zeiss confocal microscope (Zeiss, LSM 800) with a 20× or 40× objective.

Transmission electron microscopy

Vacuolated cells were prepared by treating the cells in condition A plus 14% FBS for 2 days; vesicles were produced by treating the cells in condition B (which includes 3 µM Chir) for 10 days. Sample preparation followed the specimen protocol of the National Instrumentation Center for Environmental Management (Seoul National University): Samples were fixed for 2 h in 2% paraformaldehyde and 2% glutaraldehyde and postfixed for 1 h using 2% osmium tetroxide in 0.1 M cacodylate buffer. Samples were then stained in 0.5% uranyl acetate overnight and dehydrated in a series of EtOH solutions (30, 50, 70, 80, 90 and 100%) for 10 min each. Finally, the samples were imbedded in Spurr's resin, sectioned at 70 nm with a Leica ultramicrotome (Leica, EM UC7), and photographed using a 80 kV JEOL JEM 1010 transmission electron microscope (JEOL, Tokyo).

Live-cell video imaging

To determine the fate of vacuolated cells under vacuole-inducing conditions, randomly selected cells were numbered and traced individually until death or the end of the filming period (days 1-4). The tracing graph was generated using MATLAB vR2018b software (MathWorks, Natick, MA, USA). To study the reversibility of vacuolization, vacuolated cells were collected with a glass pipette, transferred to condition A and filmed for 1-2 days. To film the transition from vacuoles to vesicles, microaggregates were collected from condition B at day 4 or 5 and cultured in the same medium for a further 1-2 days. All videos were taken at 37°C, one photo every 30 s, in a JuLI Fl live image system (JuLI-FLG04; NanoEnTek, Seoul, Korea) and edited with Adobe Premiere CS6 (Adobe Systems, San Jose, CA, USA) and Vapmix (VAPSHION, Seoul, Korea).

Microscopy

In this study, a Zeiss LSM 800 confocal microscope (Plan-Apochromat 20×/0.8 M27, C Plan-Apochromat 40×/1.30 or C Plan-Apochromat 63×/1.40) and an inverted DMIL LED/DFC295 fluorescence microscope (Hi Plan 4×/0.10, Hi Plan 10×/0.25 PH1, N Plan L 20×/0.35 PH1 or N Plan L 40×/0.55 CORR PH 2) were used with Zen software (v2.3, Zeiss) and the Leica application suite (v4.3.0, Leica), respectively. The images were improved with Photoshop CS6 (Adobe) in accordance with the journal's guidelines.

Quantitative RT-PCR

Total RNA was extracted with the Hybrid-R kit (305-101; GeneAll, Seoul, Korea). SYBR green (RT500M; Enzynomics, Daejeon, Korea) was used in combination with a reverse transcriptase kit (DR22-R10k; Solgent, Daejeon, Korea) and QuantStudio3 Real-Time PCR system (Thermo Fisher Scientific, A28572). Fold differences in transcript levels were determined with the $2^{-\Delta\Delta Ct}$ method, using *β-actin* mRNA for normalization. Primers for PCR are listed in Table S8.

RNA sequencing and bioinformatics

For RNA-seq, the rat pXEN cell line CX1 was cultured under the conditions defined in the figure legends and described in detail in the foregoing paragraphs. For each condition, samples were generated from three independent cell culture experiments, performed on different days and using different passage numbers. RNA was isolated from whole cultures, except for AP-stained cultures. To isolate AP-stained cells (considered as vacuolated), ∼1,600,000 cells (cultured in 100 mm dishes) were trypsinized and stained as described, suspended in 4 ml PBS, filtered (35 µm) and sorted with a Becton Dickinson FACSAria III cell sorter (BD Biosciences) for 30-50 min. About 4 ml PBS was used for collecting the sorted cells, which were then centrifuged and dissolved in Trizol (TAKARA, 9190) for RNA-seq analysis.

Transcriptome sequencing was performed as previously described (Kim et al., 2016). Briefly, total RNA was extracted using Trizol and the QIAGEN RNeasy Mini Kit (74104; QIAGEN, Hilden, Germany). For ribosomal RNA (rRNA) depletion, the RiboMinus Eukaryote kit (Thermo Fisher Scientific, A1083708) was used according to the manufacturer's instructions. The RNA library was prepared with the NEBNext UltraTM directional RNA library preparation kit for Illumina (E7420S; New England BioLabs, Ipswich, MA, USA). After cDNA synthesis, cDNA fragmentation and adaptor ligation, the products were purified with AMPure XP beads (Beckman Coulter, Brea, CA, USA) and amplified by PCR (15 cycles) to generate the final cDNA library. The RNA library was sequenced using the Illumina HiSeq2500 (Illumina, San Diego, CA, USA). The RNA-seq raw data underwent quality check and control using FastQC v0.11.5 (Babraham Bioinformatics, UK) and Trimmomatic v0.36 (Bolger et al., 2014). Published data on mouse embryos (E3.5-E6.5 embryos; epiblast and ExEn cells; E9.5, E12.5 and E16.5 visceral yolk sac cells) and rat pXEN cell lines were included in the bioinformatics analysis (see Table S9). Mouse and rat quality-controlled FASTQ files were aligned by STAR 2.5.3a (Dobin et al., 2013) with the UCSC reference genome (http://genome.ucsc.edu/) mm10 and rn6, respectively. The gene annotation was based on Ensembl Release 94 (http://www.ensembl.org). The integration of cross-species data was restricted to the overlapping set of genes. The data analysis was performed in RStudio v1.1383 (RStudio, Boston, MA, USA) and packages were downloaded from either CRAN (https://cran.r-project.org/web/packages) or Bioconductor (http://www.bioconductor.org). t-SNE plots were made using Rtsne. The expression matrix was produced by normalizing the combined counts of the previously published (see above) and new (current study) data using Limma-voom (Law et al., 2014), resulting in a normalized gene expression profiling data table (Table S12, related to Fig. 2B, Fig. 5B, Fig. S4B), which in turn was used for pairwise comparisons by Limma (Fig. 2A, Fig. S4A, Table S10, Table S11). Differentially expressed genes were cut by a log2 fold change of >1.5 and $P<0.05$, then GO and KEGG annotations were produced using the ClusterProfiler package (Yu et al., 2012). Heatmaps were created with the Pheatmap package; markers of the extraembryonic endoderm were selected from previous publications (Paca et al., 2012; Chuykin et al., 2013). Venn plots were created by VennDiagram.

Statistical analysis

All quantitative experiments were independently performed for the number of times indicated in the figure legends (*n* indicates the number of independent experiments). Prism 8 (GraphPad Software, La Jolla, CA,

USA) and Excel (Microsoft, Redmond, WA, USA) were used for the statistical analyses, including calculation of mean±s.e.m. (for error bars) and *P*-values using the two-tailed Student's *t*-test (for comparisons of two groups). Statistically significant differences are indicated as $*P<0.05$, $**P<0.01$, $***P<0.001$ or $^{\$}P<0.0001$.

Acknowledgements
We thank Prof. Chulhun Kang (Kyung Hee University, Korea) for providing the pH Probe 1.

Competing interests
The authors declare no competing or financial interests.

Author contributions
Conceptualization: B.B.; Methodology: M.K.; Software: Y.Z.; Validation: M.K., B.B.; Formal analysis: M.K., Y.Z.; Investigation: M.K., K.W.J., Y.G.C.; Resources: B.B.; Data curation: Y.Z.; Writing - original draft: B.B.; Writing - review & editing: B.B.; Visualization: M.K.; Supervision: B.B.; Project administration: B.B.; Funding acquisition: B.B., Y.G.C.

Funding
This study was supported by the National Research Foundation of Korea (2012R1A1A2007774 and 2011-0030049).

Data availability
RNA-seq data underlying Figs 2, 5 and Fig. S4 have been deposited in the Gene Expression Omnibus (GEO); accession number GSE123598.

Supplementary information
Supplementary information available online at
http://jcs.biologists.org/lookup/doi/10.1242/jcs.230607.supplemental

References
Adamson, E. D., Strickland, S., Tu, M. and Kahan, B. (1985). A teratocarcinoma-derived endoderm stem cell line (1H5) that can differentiate into extra-embryonic endoderm cell types. *Differentiation* **29**, 68-76. doi:10.1111/j.1432-0436.1985.tb00294.x

Anderson, K. G. V., Hamilton, W. B., Roske, F. V., Azad, A., Knudsen, T. E., Canham, M. A., Forrester, L. M. and Brickman, J. M. (2017). Insulin fine-tunes self-renewal pathways governing naive pluripotency and extra-embryonic endoderm. *Nat. Cell Biol.* **19**, 1164-1177. doi:10.1038/ncb3617

Aziz, M. and Alexandre, H. (1991). The origin of the nascent blastocoele in preimplantation mouse embryos ultrastructural cytochemistry and effect of chloroquine. *Roux Arch Dev. Biol.* **200**, 77-85. doi:10.1007/BF00637187

Bangs, F. K., Schrode, N., Hadjantonakis, A.-K. and Anderson, K. V. (2015). Lineage specificity of primary cilia in the mouse embryo. *Nat. Cell Biol.* **17**, 113-122. doi:10.1038/ncb3091

Bedzhov, I. and Zernicka-Goetz, M. (2015). Cell death and morphogenesis during early mouse development: are they interconnected? *BioEssays* **37**, 372-378. doi:10.1002/bies.201400147

Bielinska, M., Narita, N. and Wilson, D. B. (1999). Distinct roles for visceral endoderm during embryonic mouse development. *Int. J. Dev. Biol.* **43**, 183-205.

Bolger, A. M., Lohse, M. and Usadel, B. (2014). Trimmomatic: a flexible trimmer for Illumina sequence data. *Bioinformatics* **30**, 2114-2120. doi:10.1093/bioinformatics/btu170

Bryant, D. M., Roignot, J., Datta, A., Overeem, A. W., Kim, M., Yu, W., Peng, X., Eastburn, D. J., Ewald, A. J., Werb, Z. et al. (2014). A molecular switch for the orientation of epithelial cell polarization. *Dev. Cell* **31**, 171-187. doi:10.1016/j.devcel.2014.08.027

Chambard, M., Gabrion, J. and Mauchamp, J. (1981). Influence of collagen gel on the orientation of epithelial cell polarity: follicle formation from isolated thyroid cells and from preformed monolayers. *J. Cell Biol.* **91**, 157-166. doi:10.1083/jcb.91.1.157

Chuykin, I., Schulz, H., Guan, K. and Bader, M. (2013). Activation of the PTHRP/adenylate cyclase pathway promotes differentiation of rat XEN cells into parietal endoderm, whereas Wnt/beta-catenin signaling promotes differentiation into visceral endoderm. *J. Cell Sci.* **126**, 128-138. doi:10.1242/jcs.110239

Datta, A., Bryant, D. M. and Mostov, K. E. (2011). Molecular regulation of lumen morphogenesis. *Curr. Biol.* **21**, R126-R136. doi:10.1016/j.cub.2010.12.003

Davis, G. E. and Camarillo, C. W. (1996). An alpha 2 beta 1 integrin-dependent pinocytic mechanism involving intracellular vacuole formation and coalescence regulates capillary lumen and tube formation in three-dimensional collagen matrix. *Exp. Cell Res.* **224**, 39-51. doi:10.1006/excr.1996.0109

Debeb, B. G., Galat, V., Epple-Farmer, J., Iannaccone, S., Woodward, W. A., Bader, M., Iannaccone, P. and Binas, B. (2009). Isolation of Oct4-expressing extraembryonic endoderm precursor cell lines. *PLoS ONE* **4**, e7216. doi:10.1371/journal.pone.0007216

Dobin, A., Davis, C. A., Schlesinger, F., Drenkow, J., Zaleski, C., Jha, S., Batut, P., Chaisson, M. and Gingeras, T. R. (2013). STAR: ultrafast universal RNA-seq aligner. *Bioinformatics* **29**, 15-21. doi:10.1093/bioinformatics/bts635

Ebnet, K., Kummer, D., Steinbacher, T., Singh, A., Nakayama, M. and Matis, M. (2018). Regulation of cell polarity by cell adhesion receptors. *Semin. Cell Dev. Biol.* **81**, 2-12. doi:10.1016/j.semcdb.2017.07.032

Ezashi, T., Matsuyama, H., Telugu, B. P. and Roberts, R. M. (2011). Generation of colonies of induced trophoblast cells during standard reprogramming of porcine fibroblasts to induced pluripotent stem cells. *Biol. Reprod.* **85**, 779-787. doi:10.1095/biolreprod.111.092809

Farr, G. A., Hull, M., Mellman, I. and Caplan, M. J. (2009). Membrane proteins follow multiple pathways to the basolateral cell surface in polarized epithelial cells. *J. Cell Biol.* **186**, 269-282. doi:10.1083/jcb.200901021

González-Mariscal, L., Betanzos, A. and Ávila-Flores, A. (2000). MAGUK proteins: structure and role in the tight junction. *Semin. Cell Dev. Biol.* **11**, 315-324. doi:10.1006/scdb.2000.0178

Huang, T. and Rivéra-Perez, J. A. (2014). Senescence-associated beta-galactosidase activity marks the visceral endoderm of mouse embryos but is not indicative of senescence. *Genesis* **52**, 300-308. doi:10.1002/dvg.22761

Jewett, C. E. and Prekeris, R. (2018). Insane in the apical membrane: Trafficking events mediating apicobasal epithelial polarity during tube morphogenesis. *Traffic* **19**, 666-678. doi:10.1111/tra.12579

Kawamura, N., Sun-Wada, G.-H., Aoyama, M., Harada, A., Takasuga, S., Sasaki, T. and Wada, Y. (2012). Delivery of endosomes to lysosomes via microautophagy in the visceral endoderm of mouse embryos. *Nat. Commun.* **3**, 1071. doi:10.1038/ncomms2069

Kim, S. H., Das, A., Chai, J. C., Binas, B., Choi, M. R., Park, K. S., Lee, Y. S., Jung, K. H. and Chai, Y. G. (2016). Transcriptome sequencing wide functional analysis of human mesenchymal stem cells in response to TLR4 ligand. *Sci. Rep.* **6**, 30311. doi:10.1038/srep30311

Kimber, S. J. (1986). Distribution of lectin receptors in postimplantation mouse embryos at 6-8 days gestation. *Am. J. Anat.* **177**, 203-219. doi:10.1002/aja.1001770207

Kunath, T., Arnaud, D., Uy, G. D., Okamoto, I., Chureau, C., Yamanaka, Y., Heard, E., Gardner, R. L., Avner, P. and Rossant, J. (2005). Imprinted X-inactivation in extra-embryonic endoderm cell lines from mouse blastocysts. *Development.* **132**, 1649-1661. doi:10.1242/dev.01715

Law, C. W., Chen, Y., Shi, W. and Smyth, G. K. (2014). voom: precision weights unlock linear model analysis tools for RNA-seq read counts. *Genome Biol.* **15**, R29. doi:10.1186/gb-2014-15-2-r29

Lee, J. L. and Streuli, C. H. (2014). Integrins and epithelial cell polarity. *J. Cell Sci.* **127**, 3217-3225. doi:10.1242/jcs.146142

Lee, M. H., Han, J. H., Lee, J. H., Park, N., Kumar, R., Kang, C. and Kim, J. S. (2013). Two-color probe to monitor a wide range of pH values in cells. *Angew. Chem. Int. Ed. Engl.* **52**, 6206-6209. doi:10.1002/anie.201301894

Lo Nigro, A., Geraerts, M., Notelaers, T., Roobrouck, V. D., Muijtjens, M., Eggermont, K., Subramanian, K., Ulloa-Montoya, F., Park, Y., Owens, J. et al. (2012). MAPC culture conditions support the derivation of cells with nascent hypoblast features from bone marrow and blastocysts. *J. Mol. Cell Biol.* **4**, 423-426. doi:10.1093/jmcb/mjs046

Magin, T. M., McWhir, J. and Melton, D. W. (1992). A new mouse embryonic stem cell line with good germ line contribution and gene targeting frequency. *Nucleic Acids Res.* **20**, 3795-3796. doi:10.1093/nar/20.14.3795

Manninen, A. (2015). Epithelial polarity–generating and integrating signals from the ECM with integrins. *Exp. Cell Res.* **334**, 337-349. doi:10.1016/j.yexcr.2015.01.003

Maurer, M. E. and Cooper, J. A. (2005). Endocytosis of megalin by visceral endoderm cells requires the Dab2 adaptor protein. *J. Cell Sci.* **118**, 5345-5355. doi:10.1242/jcs.02650

Nemani, N., Carvalho, E., Tomar, D., Dong, Z., Ketschek, A., Breves, S. L., Jaña, F., Worth, A. M., Heffler, J., Palaniappan, P. et al. (2018). MIRO-1 Determines mitochondrial shape transition upon GPCR activation and Ca(2+) stress. *Cell Rep* **23**, 1005-1019. doi:10.1016/j.celrep.2018.03.098

Noguchi, M., Noguchi, T., Watanabe, M. and Muramatsu, T. (1982). Localization of receptors for Dolichos biflorus agglutinin in early post implantation embryos in mice. *J. Embryol. Exp. Morphol.* **72**, 39-52.

Overeem, A. W., Bryant, D. M. and van IJzendoorn, S. C. (2015). Mechanisms of apical-basal axis orientation and epithelial lumen positioning. *Trends Cell Biol.* **25**, 476-485. doi:10.1016/j.tcb.2015.04.002

Paca, A., Séguin, C. A., Clements, M., Ryczko, M., Rossant, J., Rodriguez, T. A. and Kunath, T. (2012). BMP signaling induces visceral endoderm differentiation of XEN cells and parietal endoderm. *Dev. Biol.* **361**, 90-102. doi:10.1016/j.ydbio.2011.10.013

Pozzi, A., Yurchenco, P. D. and Iozzo, R. V. (2017). The nature and biology of basement membranes. *Matrix Biol.* **57-58**, 1-11. doi:10.1016/j.matbio.2016.12.009

Rivron, N. C., Frias-Aldeguer, J., Vrij, E. J., Boisset, J.-C., Korving, J., Vivié, J., Truckenmüller, R. K., van Oudenaarden, A., van Blitterswijk, C. A. and Geijsen, N. (2018). Blastocyst-like structures generated solely from stem cells. *Nature* **557**, 106-111. doi:10.1038/s41586-018-0051-0

Shimada, A., Nakano, H., Takahashi, T., Imai, K. and Hashizume, K. (2001). Isolation and characterization of a bovine blastocyst-derived trophoblastic cell line,

BT-1: development of a culture system in the absence of feeder cell. *Placenta* **22**, 652-662. doi:10.1053/plac.2001.0702

Sigurbjörnsdóttir, S., Mathew, R. and Leptin, M. (2014). Molecular mechanisms of de novo lumen formation. *Nat. Rev. Mol. Cell Biol.* **15**, 665-676. doi:10.1038/nrm3871

Stephenson, R. O., Yamanaka, Y. and Rossant, J. (2010). Disorganized epithelial polarity and excess trophectoderm cell fate in preimplantation embryos lacking E-cadherin. *Development* **137**, 3383-3391. doi:10.1242/dev.050195

Strilić, B., Kučera, T., Eglinger, J., Hughes, M. R., McNagny, K. M., Tsukita, S., Dejana, E., Ferrara, N. and Lammert, E. (2009). The molecular basis of vascular lumen formation in the developing mouse aorta. *Dev. Cell* **17**, 505-515. doi:10.1016/j.devcel.2009.08.011

Taniguchi, K., Shao, Y., Townshend, R. F., Cortez, C. L., Harris, C. E., Meshinchi, S., Kalantry, S., Fu, J., O'Shea, K. S. and Gumucio, D. L. (2017). An apicosome initiates self-organizing morphogenesis of human pluripotent stem cells. *J. Cell Biol.* **216**, 3981-3990. doi:10.1083/jcb.201704085

van Roy, F. and Berx, G. (2008). The cell-cell adhesion molecule E-cadherin. *Cell. Mol. Life Sci.* **65**, 3756-3788. doi:10.1007/s00018-008-8281-1

Vashi, N., Andrabi, S. B., Ghanwat, S., Suar, M. and Kumar, D. (2017). Ca(2+)-dependent focal exocytosis of golgi-derived vesicles helps phagocytic uptake in macrophages. *J. Biol. Chem.* **292**, 5144-5165. doi:10.1074/jbc.M116.743047

Wada, Y. (2013). Vacuoles in mammals: a subcellular structure indispensable for early embryogenesis. *Bioarchitecture* **3**, 13-19. doi:10.4161/bioa.24126

Wang, A. Z., Ojakian, G. K. and Nelson, W. J. (1990). Steps in the morphogenesis of a polarized epithelium. I. Uncoupling the roles of cell-cell and cell-substratum contact in establishing plasma membrane polarity in multicellular epithelial (MDCK) cysts. *J. Cell Sci.* **95**, 137-151.

Wu, J. J., Avey, D., Li, W., Gillen, J., Fu, B., Miley, W., Whitby, D. and Zhu, F. (2016). ORF33 and ORF38 of Kaposi's sarcoma-associated herpesvirus interact and are required for optimal production of infectious progeny viruses. *J. Virol.* **90**, 1741-1756. doi:10.1128/JVI.02738-15

Yano, T., Kanoh, H., Tamura, A. and Tsukita, S. (2017). Apical cytoskeletons and junctional complexes as a combined system in epithelial cell sheets. *Ann. N. Y. Acad. Sci.* **1405**, 32-43. doi:10.1111/nyas.13432

Yu, G., Wang, L.-G., Han, Y. and He, Q.-Y. (2012). clusterProfiler: an R package for comparing biological themes among gene clusters. *OMICS* **16**, 284-287. doi:10.1089/omi.2011.0118

Zhong, Y., Choi, T., Kim, M., Jung, K. H., Chai, Y. G. and Binas, B. (2018). Isolation of primitive mouse extraembryonic endoderm (pXEN) stem cell lines. *Stem Cell Res.* **30**, 100-112. doi:10.1016/j.scr.2018.05.008

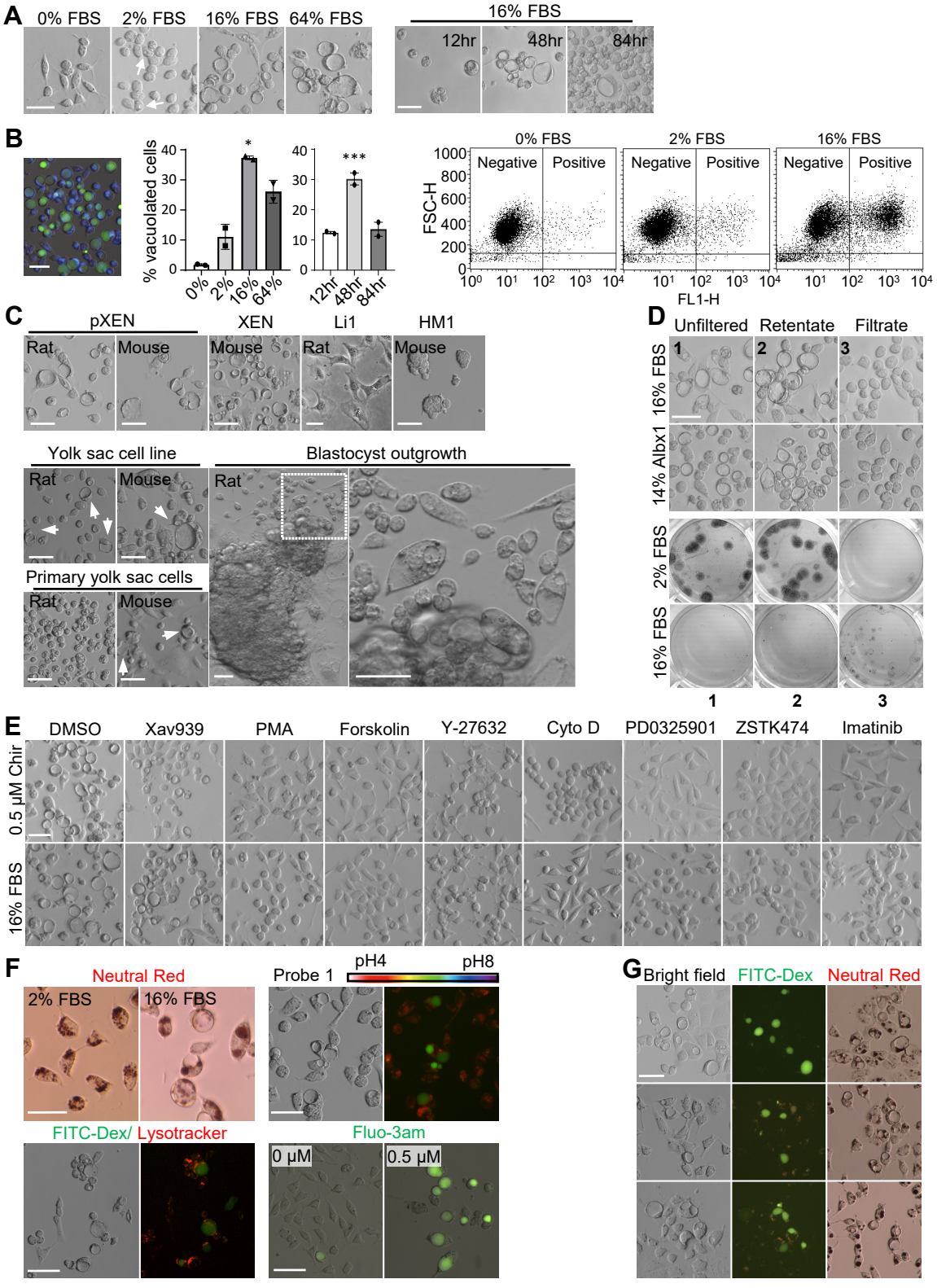

Fig. S1. Additional characterization of vacuoles and vacuolization factors. **(A)** Effects of serum concentration and culture time/cell density. Left row: Rat pXEN cells (line CX1) were cultured for 2 days in different concentrations of FBS (final concentrations: 2%, 16%, 64%); arrows indicate smaller vacuoles. Right row: Cells were cultured in 16% FBS for the indicated time points. **(B)** The proportion of vacuolated cells was quantified by flow cytometry after AP staining on Day 2. The photo illustrates the specificity of the AP dye (green: AP dye; blue: DAPI). Columns show mean ± s.e.m. from two independent experiments (n=2), each performed in duplicate. *, $p < 0.05$; ***, $p < 0.001$ (left columns: versus 2% FBS ("ground state"); right columns: versus 12 hours) by two-tailed Student's t-test. The plots show representative flow cytometry patterns. **(C)** Comparison of cell types for the propensity to vacuolate. Vacuolization tendency appeared to decrease in the order: blastocyst outgrowths > pXEN cells > XEN cells > primary yolk sac cells > yolk sac cell line; no vacuolization was observed in rat fibroblast cells (line Li1) and mouse ESCs (line HM1). E4.5 blastocysts, E12.5 dissociated yolk sacs and ExEn lineage cells, except XEN cells, were cultured in condition A with additional 14% FBS for 7 days (blastocyst), 4 days (yolk sac), or 2 days (cell lines), respectively. XEN cells, Li1, and HM1 cells were cultured for 2 days in their respective routine culture media but with additional 20% FBS. Arrow head indicates vacuole. **(D)** Vacuole-inducing capacity of serum and Albumax1 filtrate. 2% or 16% of unfiltered FBS or Albumax1, of >50 KDa retentate, and of the <50KDa filtrate were compared. Upper row: 5,000 cells were cultured for 2 days at standard cell density (for vacuole formation). Lower row: 100 cells were seeded in plating assays and analyzed after 5 days. The numbers represent each condition. **(E)** Preventive or inhibitory effects of signaling drugs on vacuolization. The drugs were present for 1 day in addition to vacuole-inducing factors (0.5 µM Chir or 16% FBS). Drug concentrations: 6 µM Xav939; 40 µM PMA; 20 µM Forskolin; 20 µM Y-27632; 65 µM Cytochalasin D (Cyto D); 50 µM PD0325901; 1 µM ZSTK474; 50 nM Imatinib. **(F)** Assessment of the intravacuolar milieu. For the pH assessments, cells were cultured with and without additional 14% FBS (final concentrations: 2 vs. 16% FBS) and then stained with Neutral Red, Probe 1, or FITC-Dextran/Lysotracker. The pH color scale for Probe 1 is taken from Lee MH et al., 2013. For the Ca assessment, cells were cultured without or with 0.5 µM of Chir, and then stained with Fluo-3am. **(G)** Assessment of vacuolar pH in vacuoles that were induced with three different drugs: 0.5 µM Chir, 1 µM Bim1, or 2 µM Gö6983. pH was assessed by incubation with FITC-Dextran or Neutral Red on Day 2. Scale bars, 50 µm (A-G). All photos represent at least two independent experiments. Except for (D), the experiments were based on condition A. FITC-Dex, FITC-Dextran. Albx1, Albumax1.

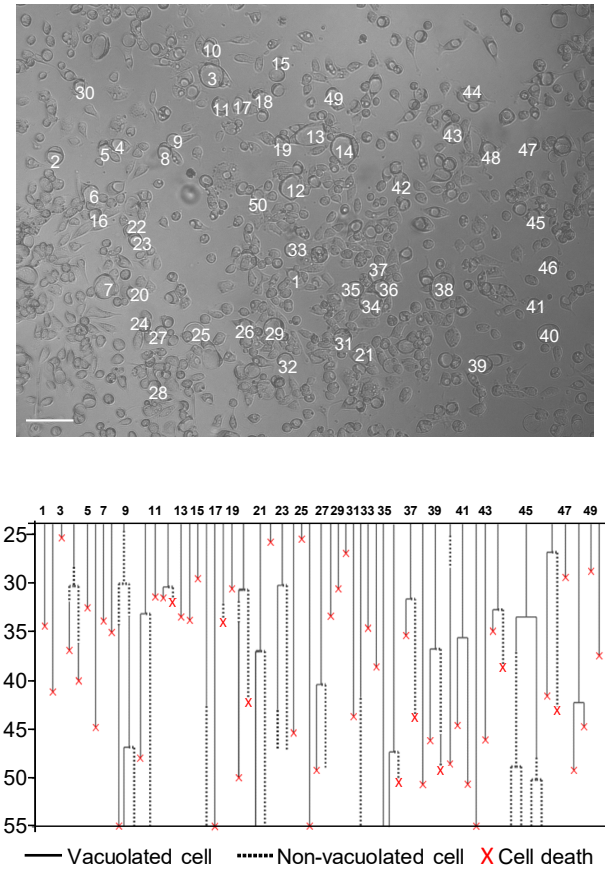

Fig. S2. Fate of vacuolated cells. 50 cells were tracked in condition A with additional 14% FBS on live cell imager from 48 to 80 hours (Video SV5). Scale bar, 100 µm.

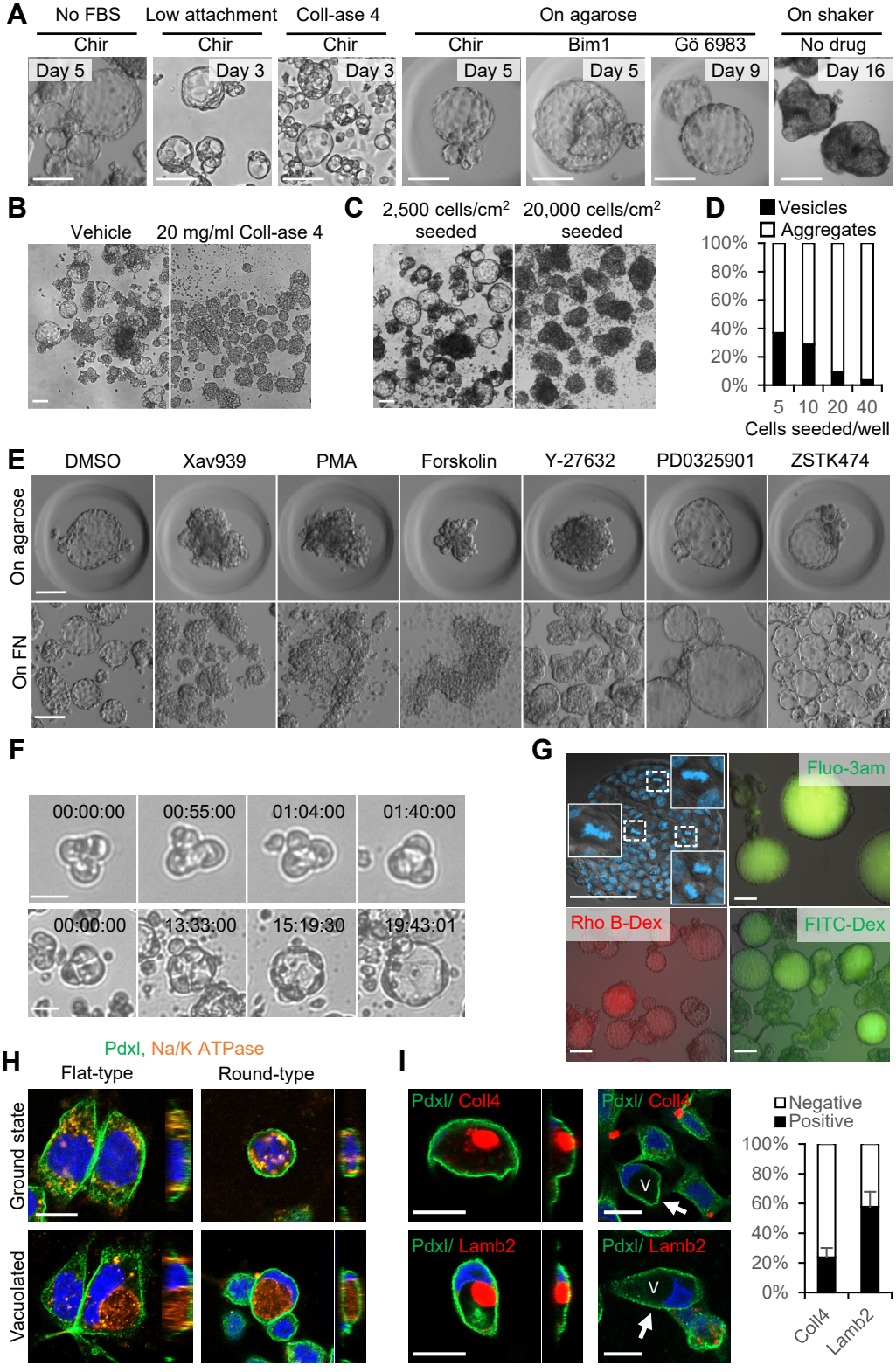

Fig. S3. Additional characterization of vesicle-producing cultures. **(A)** Comparison of vesicle-inducing conditions. pXEN cells were cultured for the indicated times under condition A, but with the indicated modifications (including no FBS instead of 2% FBS; low attachment plastic plates or agarose microwells instead of fibronectin-coated plastic plates; on shaker instead of non-moving plates) and in the additional presence of the indicated drug (3 µM Chir, 3 µM Bim1, 5 µM Gö 6983) or of collagenase 4 (0.1 mg/ml). Scale bars, 100 µm (except on shaker), 300 µm (on shaker). **(B)** Treatment with a high collagenase 4 concentration prevents vesiculation and instead causes aggregation. Cells were cultured in 4-well plates under condition B. Scale bar, 100 µm. The photos are representative of 3 independent experiments. **(C)** High cell density prevents vesiculation and instead causes aggregation. Cells were cultured in 4-well plates under condition B. Scale bar, 100 µm. The photos are representative of 3 independent experiments. **(D)** High cell density prevents vesiculation and instead causes aggregation. Cells were cultured in agarose microwells under condition A + 3 µM Chir. Numbers are based on 2 independent experiments. **(E)** Inhibitory effects of some signaling drugs on vesicle formation. Vesicles were formed over 5 days in condition A plus 3 µM Chir or condition B (which already includes 3 µM Chir). Cells were cultured in 3% agarose microwells for condition A and on fibronectin-coated wells for condition B. 3 µM Xav939; 20 µM PMA; 20 µM Forskolin; 40 µM Y-27632; 50 µM PD0325901; 1 µM ZSTK474. Scale bars, 100 µm. **(F)** Movie images showing one example of transition from vacuolar to vesicular lumen (see Videos SV9 and 10). 3 vacuolated cells formed one lumen (top) and kept growing (bottom). hr:min:sec. Scale bar, 25 µm (top), 50 µm (bottom). **(G)** Expansion of vesicles. Shown are vesicles stained with DAPI (boxes: mitotic chromosomes) or photographed after incubation with Fluo-3am, Rho B-Dextran, or FITC-Dextran. Scale bars, 100 µm. **(H)** Top and side views of “ground state” and vacuolated pXEN cells stained for Pdxl and Na/K ATPase. Note that in rounded but not flat cells, Pdxl is also present in the bottom part of the plasma membrane. The photos represent three independent experiments. Blue, nuclei (DAPI stain). **(I)** Photos: Top and side views of vacuolated pXEN cells immunostained for Pdxl, collagen 4, and laminin B2. The photos show examples of vacuoles that are filled with laminin or collagen (left) or free of these proteins (right). Columns: Percentages of collagen 4-positive or laminin B2-positive vacuoles at the vacuolated stage. V and arrows indicate vacuoles. Scale bars, 20 µm (H, I). Mean±s.e.m. from 5 independent experiments.

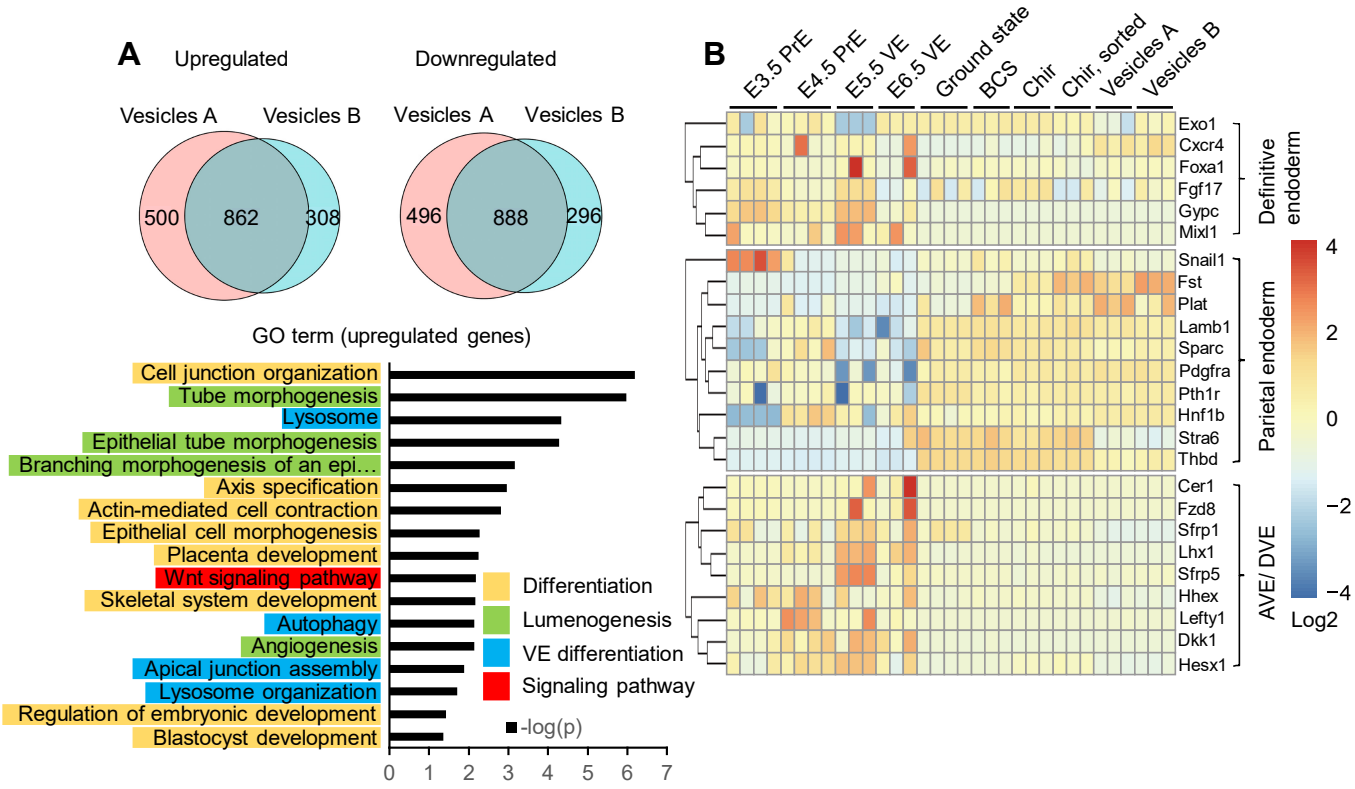

Fig. S4. Transcriptome analysis of vesiculation. **(A)** Comparison of normal pXEN cells with "Vesicles A" (condition A plus 3 µM Chir) and "Vesicles B" (condition B, which already includes 3 µM Chir). Top, Venn diagrams. Bottom, Gene ontology of biological annotation; same colors indicate related meanings (see color legend). See also Tables S10 and S11. **(B)** Heatmap comparison of definitive endoderm, parietal endoderm, anterior visceral endoderm (AVE)/ distal visceral endoderm (DVE) marker gene expression in "ground state" (condition A= maintenance condition) pXEN cells, vacuolated pXEN cells, pXEN cell-derived vesicles, and related in vivo samples. **(C)** Immunostainings showing disappearance of the pluripotency marker Oct4, but maintenance of the PrE marker Gata4, during vacuolization and vesicular morphogenesis of pXEN cells. **(D)** Epithelial morphologies of immature (Vesicles B; with Chir) and more mature (Mature vesicles B; Chir withdrawn) vesicles. Images in (C) and (D) were obtained with a confocal microscope. Scale bars, 20 µm. All photos represent at least two independent experiments.

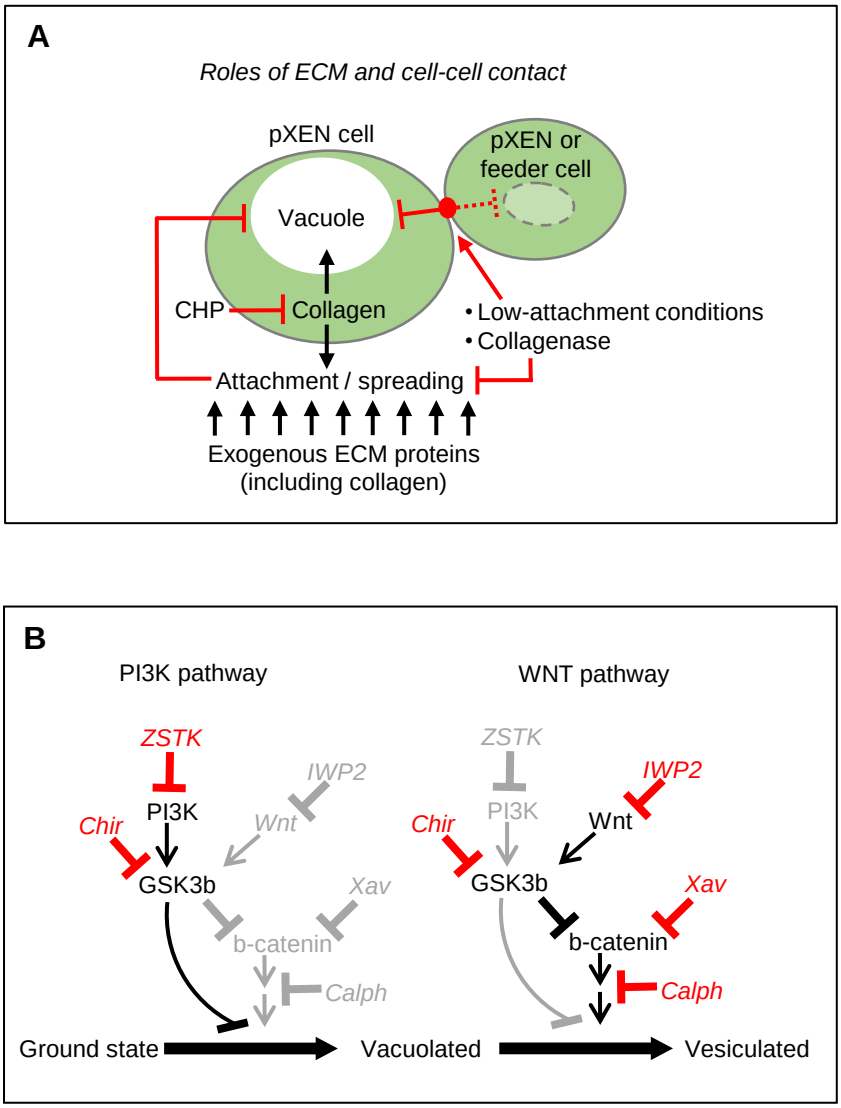

Fig. S5. Control mechanisms of vesicular morphogenesis. **(A)** Schematic summarizing control of vacuolization. pXEN cells have an inherent tendency to create vacuoles, which is held in check by ECM proteins (notably including self-synthesized collagen) and by cell-cell contact. Note that endogenously synthesized collagen can be secreted both out of the cell and into vacuoles, although not necessarily at the same time. **(B)** Potential roles of PI3K and Wnt pathways. Only the results obtained with drugs that are directly relevant to those pathways are included. Each drug was tested both in the vacuolization and in the vesiculation stage. Drugs that showed effects are depicted in red color. When a drug showed no effect, it is depicted in grey color. Full drug names, see Materials and Methods.

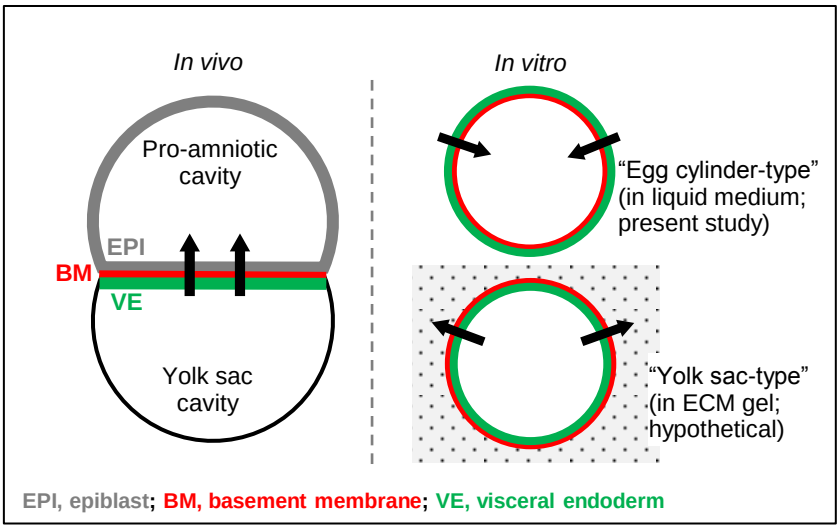

Fig. S6. Schematic explaining relationship of VE-like vesicles with egg cylinder. It depends on the function studied whether a vesicle is "in vivo-like". **Left**, Schematic of the egg cylinder-stage embryo with distorted proportions to emphasize topology (for a schematic of the egg cylinder with realistic proportions, see Fig. 6B). Also shown is the transport function of the early VE (arrow), which is executed in tandem with the epiblast. The schematic ignores that later the pro-amniotic cavity also extends into the extraembryonic ectoderm, but this does not alter the notions discussed. **Right**, Depending on their orientation, VE vesicles represent different functions of the VE in vitro. For transport studies, "egg cylinder-type" VE vesicles (present study) are more in vivo-like, as the yolk sac cavity is the "outside". Such vesicles are also more practical, as they do not need pre-loading. "Yolk sac-type" VE vesicles were not produced in the present study but probably are feasible when using an ECM gel.

Table S1. Chemicals, culture additives, growth factors

Product	Company	Catalog No.
0.05% trypsin/ EDTA	Welgene, Gyeongsan, Korea	LS015-09
A83-01	Peprotech, RI, U.S.	9094360
Advanced DMEM/F12	ThermoFisher, Waltham, MA, U.S.	12634-010
Albumax1	ThermoFisher	11020-021
Ascorbic acid	Sigma, St. Louis, MO. U.S.	A8960
B27 supplement without vitamin A	ThermoFisher	12587-010
β-mercaptoethanol	Sigma	M7522
BCS	Welgene	S003-05
Bovine fibronectin	ThermoFisher	33010018
Crytal violet	Sigma	C.I. 42555
DMEM (high glucose)	Sigma	D6429
DMEM (low glucose)	Sigma	D6046
DMEM/F12	ThermoFisher	21331-020
Donkey serum	Genetex, Irvine, CA U.S.	GTX73205
EGF	Miltenyi Biotec, Bergisch Gladbach, Germany	130-093-825
Fatty acid-free BSA	GenDEPOT, Katy, TX, U.S.	A0100-010
FBS	MP biomedicals, Santa Ana, CA, U.S.	2916754 (Lot# M6164)
Fraction V BSA	Roche, Basel, Switzerland	10774111103
Glutamax	ThermoFisher	35050061
Hybrid-R (RNA extraction)	GeneAll, Seoul, Korea	305-101
ITS	ThermoFisher	41400
Knockout serum replacement	ThermoFisher	10828-010
LA-BSA	Sigma	L9530
LIF	ORF Genetics, Kopavogur, Iceland	01-A1140
MCDB-201	Sigma	M6770
Mitomycin C	Tocris, Bristol, UK	3258
N2 supplement	ThermoFisher	17502-048
N-acetylcysteine	Sigma	A7250
Neurobasal	ThermoFisher	21103-049
Paraformaldehyde	JUNSEI, Tokyo, Japan	58295-1201
PDGF	ThermoFisher	14-8501-80
Penicillin/ streptomycin	ThermoFisher	10378016
Polyethylenimine (PEI) system	Polyscience, Warrington, PA, U.S.	23966
Propidium iodide	Sigma	P4170
Puromycin	Invivogen, Pak Shek Kok, Hong Kong	ant-pr-1
Random hexamer	Enzynomics, Daejeon, Korea	N101M
Reverse transcriptase kit	Solgent, Daejeon, Korea	DR23-R10k
RNAse A	m.biotech, Hanam, Korea	43014
SYBR green	Enzynomics	RT500M

Triton X-100	Fisher Scientific, Hampton, NH, U.S.	T/3751/08
Trizol	TAKARA, Kusatsu, Japan	9109
Vectashield	Vector Laboratories, Burlingame, CA, U.S.	H-1000

Table S2. Molecules tested for effects on vacuolization and vesiculation

Drug	Catalog No.	Company
Bisindolylmaleimide 1 (Bim1)	B-6191	LC laboratories, Woburn, MA, U.S.
Calphostin C	AG-CN2-0430-C100	Adipogen, San Diego, CA, U.S.
Chir99021	4423	Tocris
Cytochalasin D	1233	Tocris
Forskolin	1099	Tocris
Gö6983	G-7700	LC laboratories
Imatinib	I-5508	LC laboratories
IWP2	6866167	Peprotech
PD0325901	4192	Tocris
PMA (Phorbol 12-myristate 13-acetate)	P-1680	LC laboratories
XAV939	13596	Cayman, Ann Arbor, MI, U.S.
Y-27632	A3008	Apexbio, Boston, MA, U.S.
ZSTK474	S1072	Selleck, Houston, TX, U.S.
cis-L-hydroxy-proline (CHP)	H1169	Tokyo chemical, Nihonbashi-honcho, Tokyo, Japan
Collagenase 4 (Coll-ase 4)	LS004186	Worthington, Lakewood, NJ, U.S.

Table S3. Composition of media

Culture condition	Media components	Application
A	Low glucose DMEM, MCDB, 1% (v/v) penicillin/streptomycin, 1x (v/v) LA-BSA, 1x (v/v) ITS, 0.1 nM L-ascorbic acid, 2% (v/v) FBS, 0.5 µM Dexamethasone, 10 ng/ml PDGF, 10 ng/ml EGF, 10 ng/ml LIF, 55 µM β-mercaptoethanol, 100 ng/ml fibronectin	Routine culture condition for rat and mouse pXEN and yolk sac stem cell culture
B	DMEM/F12, Neurobasal, 1x (v/v) N2, 1x (v/v) B27, 1% (v/v) penicillin/streptomycin, 1x (v/v) Glutamax, 10 ng/ml LIF, 100 µM β-mercaptoethanol, 3 µM Chir99021	Vesicle and duct formation
C	Advanced DMEM/F12, 1x (v/v) N2, 1x (v/v) B27, 1% (v/v) penicillin/streptomycin, 1x (v/v) Glutamax, 1.25 mM N-acetylcysteine, 50 ng/ml EGF, 500 nM A83-01	Differentiation of vesicles
XEN cells	70% (v/v) conditioned medium (three days on Mitomycin C treated MEF) with 30% (v/v) fresh medium (RPMI 1640 (Sigma, R0883), 20% (v/v) FBS, 1% (v/v) penicillin/streptomycin, 1 mM sodium pyruvate (Sigma, P5280), 2 mM L-glutamine (Sigma, G8540))	Observation of vacuoles
Li1 cells	High glucose DMEM, 1% (v/v) penicillin/streptomycin, 7.5% (v/v) FBS	Feeder cells or control cells
HM1 cells	High glucose DMEM, 1% (v/v) penicillin/streptomycin, 15% (v/v) FBS, 10 ng/ml LIF, 100 µM β-mercaptoethanol, 0.1% gelatin	Control cells

Table S4. Organisms/strains

Species (organ)	Sex	Strain	Age	Company
Mouse (Yolk sac)	Female	ICR	12 weeks	Koatech, Pyeongtaek, Korea
Rat (Blastocyst)	Female	SD	11 weeks	Koatech
Rat (Yolk sac)	Female	SD	10 weeks	Koatech

Table S5. Cell lines

Cell line	Species	Strain	Sex	Reference
CX1 (RX1)	rat	WKY	M	Debeb et al., 2009, Zhong et al., 2018
HM1	mouse	129	M	Magin et al., 1992
Li1	rat	SD	F	Debeb et al., 2009
MAX3	rat	F344	M	Zhong et al., 2018, Lo Nigro et al., 2012
pXEN6	mouse	ICR	F	Zhong et al., 2018
XEN5	mouse	ICR	M	Zhong et al., 2018

Table S6. Organelle markers

Plasmid	Target	Company	Catalog No.
B4GALT1-pmTurquoise2	Golgi	Addgene, Watertown, MA, U.S.	36205, RRID: Addgene_36205
COX8A-pmTurquoise2	Mitochondria		36208, RRID: Addgene_36208
Lamp1-RFP	Lysosome		1817, RRID: Addgene_1817
Sec61-mCh	ER		49155, RRID: Addgene_49155
Rab5-mRFP	Eary endosome		14437, RRID: Addgene_14437
Rab7-GFP	Late endosome		12605, RRID: Addgene_12605

Table S7. Antibodies, phalloidin, DBA

	Target	Company	Catalog No.	Dilution	Host
1st	Afp (Alpha-fetoprotein)	Cusabio, Houston, TX, U.S.	CSB-PA001421LA01MO, RRID: Not found	1:200	Rabbit
1st	Cdh1 (E-cadherin)	Bioss, Woburn, MA, U.S.	bs-10009R, RRID: Not found	1:200	Rabbit
1st	Cer1 (Cerberus 1)	Santa Cruz, Dallas, TX, U.S.	sc-515324, RRID: Not found	1:200	Mouse
1st	Collagen4 (type 4 collagen)	Hybridoma bank	M3F7, RRID: AB_528167	1:200	Mouse
1st	DBA (Dolichos biflorus agglutinin)	Vector lab	RL-1032, RRID: AB_2336396	1:100	N/A
1st	Gata4 (GATA Binding Protein 4)	Santa Cruz	sc-9053, RRID: AB_2247396	1:100	Rabbit
1st	Lamb2 (Laminin, beta 2)	Hybridoma bank, IA, U.S.	D18, RRID: AB_2281095	1:200	Mouse
1st	Lrp2 (Low density lipoprotein-related protein 2)	Hybridoma bank	20B megalin, RRID: AB_2753214	1:200	Mouse

1st	Oct4 (octamer-binding transcription factor 4)	Santa Cruz	sc-5279, RRID: AB_628051	1:100	Mouse
1st	Fluorescent Dye 594-I Phalloidin	Abnova, Taipei, Taiwan	A10200, RRID: Not found	1:10000	N/A
1st	Pdxl (Podocalyxin)	Abclonal, Woburn, MA, U.S.	bs-1345R, RRID: AB_2757722	1:200	Rabbit
1st	Na/K ATPase	Hybridoma bank	A6F, RRID: AB_528092	1:100	Mouse
1st	Na/K ATPase	Abclonal	A7878, RRID: AB_2768499	1:100	Rabbit
1st	Zo-1	Biorbyt, Cambs, UK	orb340146 RRID: Not found	1:200	Rabbit
2nd	anti-mouse Alexa 488	Jackson Immunoresearch, West Grove, PA, U.S.	715-545-150, RRID: AB_2340846	1:200	Donkey
2nd	anti-rabbit DyLight 488	Bethyl, Montgomery, TX, U.S.	A120-108D2, RRID: AB_10634082	1:200	Donkey
2nd	anti-mouse DyLight 594	Bethyl	A90-337D4, RRID: AB_10630877	1:200	Donkey

Table S8. Primers used for quantitative RT-PCR

Primer name	**Forward primer (5'→3')**	**Reverse primer (5'→3')**	**Product size (bp)**	**Species**
beta-actin	CCTGGGTATGGAATCCTGTG	AGCAATGATCTTGATCTTCATGG	196	Rat and Mouse
Oct4	GAGGGATGGCATACTGTGGAC	GGTGTACCCCAAGGTGATCC	272	
Gata4	GTGCCAACTGCCAGACTACC	CCTCCTTCCGCATTGCAAGA	282	
Gata6	CATCATCACCACCCGACCTA	GCTGAGGCCGTTCATCTTACT	282	
Sox17	GAACCCGGATCTGCACAACG	CTTCTCCGCCAAGGTCAACG	76	
Sox7	GAGAGGAAACGTCTGGCAGT	CTGCCTCATCCACATAGGGC	121	
Occludin	GGCCTTTTGAGAGTCCACCT	AAAGAGTATGCCGGCTGAGA	127	
Cdh1	AAGGGCTTGGATTTTGAGG	AAATGGGGGCTTCATTCAC	139	
Ihh	CCTGTCAGCTGTAAAGCCAGG	GGAGCATAGGACCCAAGGG	336	
Epcam	GAGTCCTTGTTCCATTCAT	TCTCCTTTATCTCAGCCTTC	250	
Cited1	CCACTAGCCCCTCTGGATCA	AGCCCCTTGGTACTGGCTAT	146	
Lrp2	GCAGAGATGGACAGTGAGGT	GCTGGCGAGGCTATACG	175	
Cer1	TTGCTTTGGGAAATGCGGTT	GTGCGTGGTGGTGAATTTGG	100	
Lefty1	CTTGATCGACCGCCAGTCTTG	CTGCCACCTCTCGAAAGTTCT	151	
Otx2	TCTTCATGCGGGAGGAGGTA	TCTGACCTCCGTTCTGTTGC	123	
Afp	GCCCAGCATATGAAGAAAACA	TCTCTTTGTCTGGAAGCATTCCT	176	
Ttr	TGGACACCAAATCGTACTGG	GATGGTGTAGTGGCGATGA	104	
Apoa4	CCCAGCTAAGCAACAATGCC	CATCATGTTGGCCCGTAGGT	236	
Krt19	CTAATGGCGAGCTGGAGGTGAAG	GGCGGGCATTGTCGATCTGTAGGA	168	Rat only
Hnf4a	GAGTTTGAAAATGTGCAGGTGTTGAC	GCTGTTGGATGAGTTGAGGTTG	81	
Zo1	GCGGGCTACCTTATTGAATG	GTCATGGGAGCGAACTGAAT	124	
Apoa1	AGGGTGAAGGATTTCGCCAC	CTGTTCCTGTAGGCGACCAA	162	
ApoB	TGGAGAACTGACTGCACACG	CCCTCCAAGTCCCAAAGTCC	276	

Table S9. Published gene expression profiling data downloaded from GEO database

Accession No.	Source	Cell type	Plat-form	Species
SRX2963215	https://www.ncbi.nlm.nih.gov/sra/SRX2963215	E3.5 Epiblast	RNA-seq	Mouse
SRX2963247	https://www.ncbi.nlm.nih.gov/sra/SRX2963247		RNA-seq	Mouse
SRX2963257	https://www.ncbi.nlm.nih.gov/sra/SRX2963257		RNA-seq	Mouse
SRX2963266	https://www.ncbi.nlm.nih.gov/sra/SRX2963266		RNA-seq	Mouse
SRX2963325	https://www.ncbi.nlm.nih.gov/sra/SRX2963325	E4.5 Epiblast	RNA-seq	Mouse
SRX2963353	https://www.ncbi.nlm.nih.gov/sra/SRX2963353		RNA-seq	Mouse
SRX2963356	https://www.ncbi.nlm.nih.gov/sra/SRX2963356		RNA-seq	Mouse
SRX2963362	https://www.ncbi.nlm.nih.gov/sra/SRX2963362		RNA-seq	Mouse
SRX2963469	https://www.ncbi.nlm.nih.gov/sra/SRX2963469	E5.5 Epiblast	RNA-seq	Mouse
SRX2963478	https://www.ncbi.nlm.nih.gov/sra/SRX2963478		RNA-seq	Mouse
SRX2963490	https://www.ncbi.nlm.nih.gov/sra/SRX2963490		RNA-seq	Mouse
SRX2963498	https://www.ncbi.nlm.nih.gov/sra/SRX2963498		RNA-seq	Mouse
SRX2963686	https://www.ncbi.nlm.nih.gov/sra/SRX2963686	E6.5 Epiblast	RNA-seq	Mouse
SRX2963796	https://www.ncbi.nlm.nih.gov/sra/SRX2963796		RNA-seq	Mouse
SRX2963808	https://www.ncbi.nlm.nih.gov/sra/SRX2963808		RNA-seq	Mouse
SRX2963827	https://www.ncbi.nlm.nih.gov/sra/SRX2963827		RNA-seq	Mouse
SRX2963225	https://www.ncbi.nlm.nih.gov/sra/SRX2963225	E3.5 Primitive endoderm	RNA-seq	Mouse
SRX2963238	https://www.ncbi.nlm.nih.gov/sra/SRX2963238		RNA-seq	Mouse
SRX2963241	https://www.ncbi.nlm.nih.gov/sra/SRX2963241		RNA-seq	Mouse
SRX2963267	https://www.ncbi.nlm.nih.gov/sra/SRX2963267		RNA-seq	Mouse
SRX2963315	https://www.ncbi.nlm.nih.gov/sra/SRX2963315	E4.5 Primitive endoderm	RNA-seq	Mouse
SRX2963319	https://www.ncbi.nlm.nih.gov/sra/SRX2963319		RNA-seq	Mouse
SRX2963326	https://www.ncbi.nlm.nih.gov/sra/SRX2963326		RNA-seq	Mouse
SRX2963346	https://www.ncbi.nlm.nih.gov/sra/SRX2963346		RNA-seq	Mouse
SRX2963467	https://www.ncbi.nlm.nih.gov/sra/SRX2963467	E5.5 Visceral endoderm	RNA-seq	Mouse
SRX2963481	https://www.ncbi.nlm.nih.gov/sra/SRX2963481		RNA-seq	Mouse
SRX2963506	https://www.ncbi.nlm.nih.gov/sra/SRX2963506		RNA-seq	Mouse
SRX2963699	https://www.ncbi.nlm.nih.gov/sra/SRX2963699	E6.5 Visceral endoderm	RNA-seq	Mouse
SRX2963705	https://www.ncbi.nlm.nih.gov/sra/SRX2963705		RNA-seq	Mouse
SRX2963787	https://www.ncbi.nlm.nih.gov/sra/SRX2963787		RNA-seq	Mouse
SRX1479560	https://www.ncbi.nlm.nih.gov/sra/SRX1479560	E9.5 Visceral yolk sac	RNA-seq	Mouse
SRX1479561	https://www.ncbi.nlm.nih.gov/sra/SRX1479561		RNA-seq	Mouse
SRX1479562	https://www.ncbi.nlm.nih.gov/sra/SRX1479562		RNA-seq	Mouse
SRX1479563	https://www.ncbi.nlm.nih.gov/sra/SRX1479563		RNA-seq	Mouse
SRX1479564	https://www.ncbi.nlm.nih.gov/sra/SRX1479564		RNA-seq	Mouse
SRX1479565	https://www.ncbi.nlm.nih.gov/sra/SRX1479565		RNA-seq	Mouse

SRX1479566	https://www.ncbi.nlm.nih.gov/sra/SRX1479566	E12.5 Visceral yolk sac	RNA-seq	Mouse
SRX1479567	https://www.ncbi.nlm.nih.gov/sra/SRX1479567		RNA-seq	Mouse
SRX1479568	https://www.ncbi.nlm.nih.gov/sra/SRX1479568	E16.5 Visceral yolk sac	RNA-seq	Mouse
SRX1479569	https://www.ncbi.nlm.nih.gov/sra/SRX1479569		RNA-seq	Mouse
SRX1479570	https://www.ncbi.nlm.nih.gov/sra/SRX1479570		RNA-seq	Mouse
SRX1479571	https://www.ncbi.nlm.nih.gov/sra/SRX1479571		RNA-seq	Mouse
SRX3325623	https://www.ncbi.nlm.nih.gov/sra/SRX3325623	pXEN cells (ground state)	RNA-seq	Rat
SRX3325624	https://www.ncbi.nlm.nih.gov/sra/SRX3325624		RNA-seq	Rat
SRX3325625	https://www.ncbi.nlm.nih.gov/sra/SRX3325625		RNA-seq	Rat
SRX3325626	https://www.ncbi.nlm.nih.gov/sra/SRX3325626		RNA-seq	Rat

Table S10 A. Overlapped upregulated genes of three versions of vacuolated rat pXEN cells (BCS-treated; Chir-treated; Chir-treated and AP-sorted) (related to Fig.2A, upper left)
B. Overlapped downregulated genes of three versions of vacuolated rat pXEN cells (BCS-treated; Chir-treated; Chir-treated and AP-sorted) (related to Fig.2A, upper right)
C. Overlapped upregulated genes of two versions of rat pXEN vesicles (serum-treated; serum free) (related to Fig.S4A, upper left)
D. Overlapped downregulated genes of two versions of rat pXEN vesicles (serum-treated; serum free) (related to Fig.S4A, upper right)

Click here to Download Tables S10A-D

Table S11 A. Functional annotation of vacuolization-associated rat pXEN cell genes, identified by comparison with the ground state ($p < 0.002$) (related to Fig.2A, bottom)
B. Functional annotation of vesiculation-associated rat pXEN cell genes, identified by comparison with the ground state ($p < 0.004$) (related to Fig.S4A, bottom)

Click here to Download Tables S11A-B

Table S12. Normalized gene expression profiling data.

Click here to Download Table S12

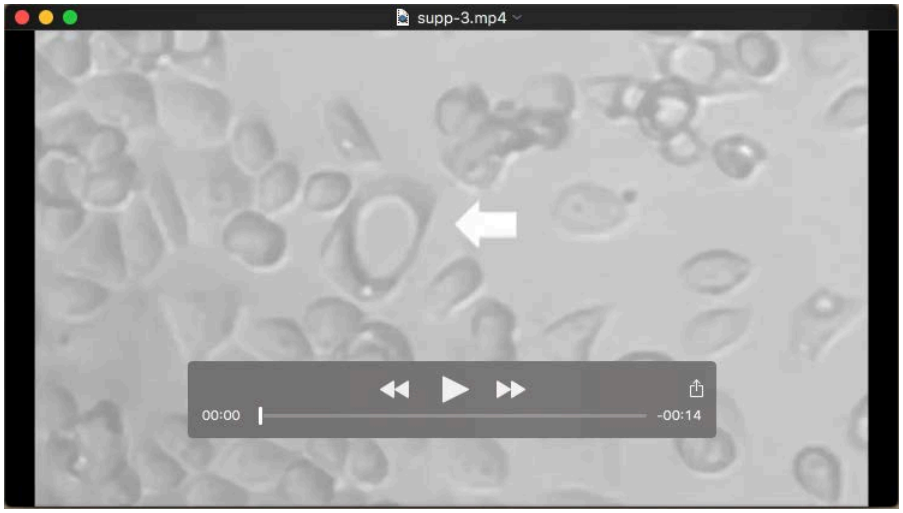

Movie 1. Reversal of vacuolization by cell-cell contact. It is shown how a single vacuolated cell (arrow) loses its vacuole when coming into contact with several non-vacuolated cells. The movie was taken 48 hours after adding 16% FBS.

Movie 2. Intracellular fusion of vacuoles. Movie shows that in a single cell (arrow), 3 vacuoles merged into one. This movie relates to Fig. 1J.

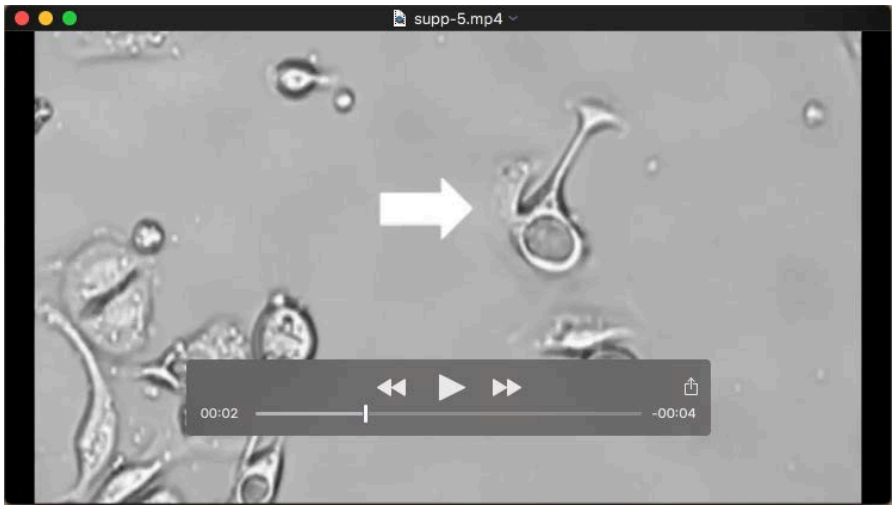

Movie 3. Reversibility of vacuolization by transfer into low-serum condition. Arrow indicates affected cell. This movie is related to Fig. 3B.

Movie 4. Aberrant cytokinesis and death of a vacuolated cell. Arrow indicates cell of interest. This movie is related to Fig. 3D.

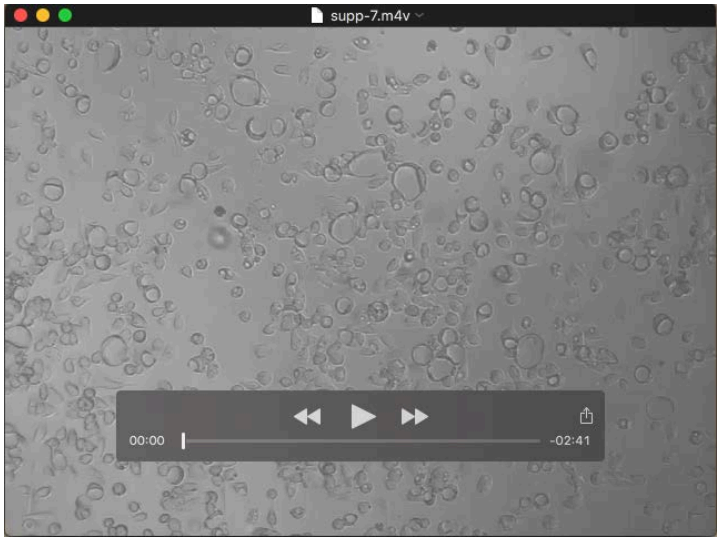

Movie 5. Population analysis (50 cells) of vacuolated cell fates. This movie is related to Fig. S2.

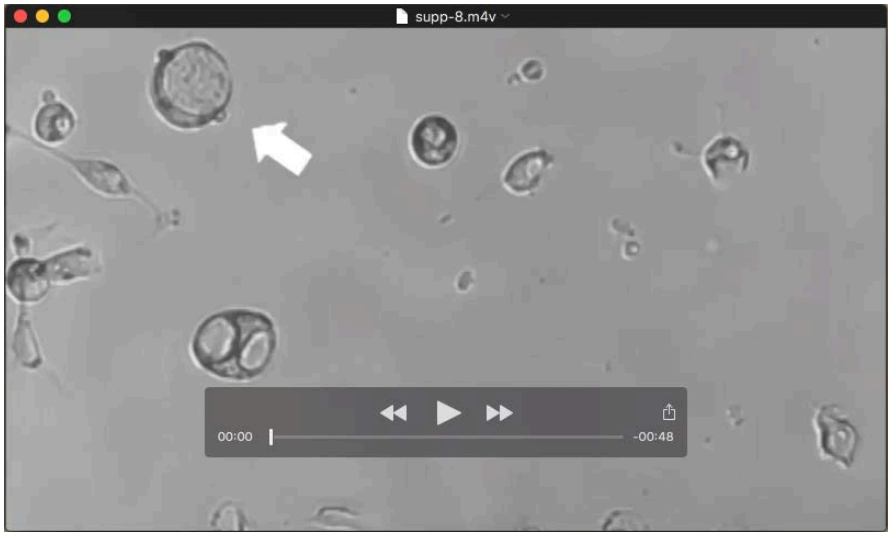

Movie 6. Patterns of cell division in surviving vacuolated cells: Type 1. This movie is related to Fig. 3E (top). Arrow indicates mother cell and arrow head indicates daughter cell.

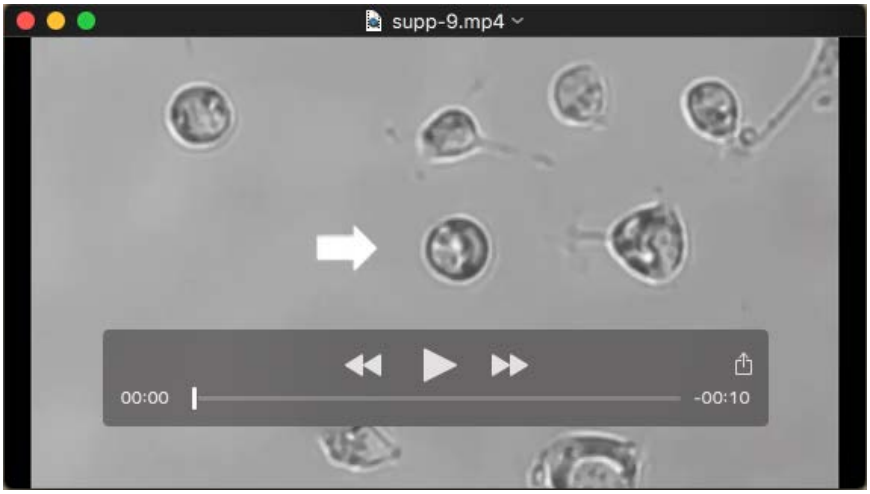

Movie 7. Patterns of cell division in surviving vacuolated cells: Type 2. This movie is related to Fig. 3E (middle). Arrow indicates cell of interest.

Movie 8. Patterns of cell division in surviving vacuolated cells: Type 3. This movie is related to Fig. 3E (bottom). Arrow indicates cell of interest.

Movie 9. Formation of nascent vesicle. It is shown how 3 vacuolated cells that are in contact produce a single lumen from the vacuoles. This movie is related to Fig. S3F (top). The arrow indicates the microaggregate of interest.

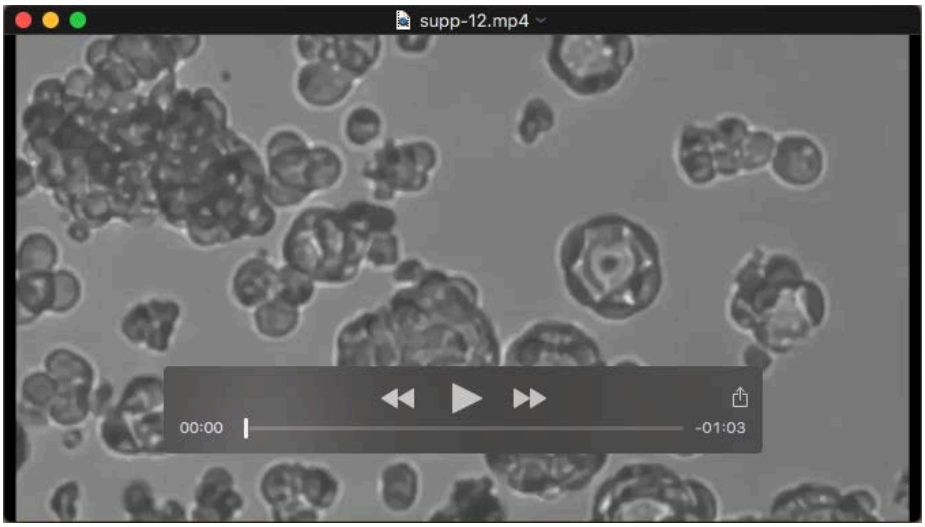

Movie 10. Expansion of vesicle. The movie shows how, starting from the 3-cell stage, the vesicle is expanding in size and cell number. This movie is related to Fig. S3F (bottom). The arrow indicates the vesicle of interest.